



SPS30 and SEN55 PM_{2.5} sensor intercomparison and validation through indoor and outdoor measurements in Arba Minch, Ethiopia

Johannes Dirk Dingemane^{1,2}, Israel Gebresilasie Kimo³, Awel Haji Ibrahim³, Yared Godine Demeke³, Nazrawit Samuel Kalbe³, Christina Isaxon^{2,*}, Axel C. Eriksson^{2,*}

5 ¹Faculty of Water Supply and Environmental Engineering, Arba Minch University, Arba Minch, Ethiopia

²Department of Design Sciences, Lund University, Lund, 221 00, Sweden

³Faculty of Meteorology and Hydrology, Arba Minch University, Arba Minch, Ethiopia

*Contributed equally

Correspondence to: Johannes Dirk Dingemane (johannesdirk.dingemane@amu.edu.et)

10 Abstract

Ethiopian air pollution is understudied yet highly relevant considering population size and source abundance including solid fuel cooking, small scale waste burning and vehicle fleet. Low cost PM_{2.5} sensors can be used to mitigate this by mapping pollution exposure. We report on indoor and outdoor measurements with Sensirion sensors SPS30 and SEN55, the former extensively validated in literature, the latter not. We evaluate their use in Arba Minch, population ca 200.000. In addition to sensor inter and intra comparison we benchmark the low-cost sensors against gravimetry. Furthermore, a separate Swedish outdoor dataset is included to extend the range of particle types and loadings and evaluate relative humidity (RH) effects using a reference-equivalent monitor (Palas FIDAS).

15 We found that the SEN55 consistently reports values 6-10 % higher than the SPS30; once this systematic offset is corrected, the sensor types are functionally identical with high precision (coefficient of variation ≤ 7.7 %, between-sampler uncertainty $\leq 1.7 \mu\text{g m}^{-3}$). Both sensors demonstrated high stability across repeated high-concentration events ($> 1000 \mu\text{g m}^{-3}$). While the SEN55 exhibits digital truncation at $6553.4 \mu\text{g m}^{-3}$, we find that measurements beyond the $1000 \mu\text{g m}^{-3}$ manufacturer specification remain meaningful and essential for accurate mass estimation in biomass-burning environments. The impact of relative humidity was small and consistent across both sensor types.

20 Our study shows that the SPS30 and SEN55 – when calibrated under circumstances of use – are stable and accurate instruments (indoor and outdoor accuracy error ≤ 22 %, outdoor expanded uncertainty ≤ 15 % in comparison to gravimetric measurements). Pragmatic, large-scale low-cost monitoring supported by mobile gravimetric validation offers the most viable path toward mitigating air pollution exposure in resource-constrained settings.

Keywords: low-cost sensors; biomass burning; gravimetry; digital truncation; Sub-Saharan Africa; resource-limited settings



1 Introduction

30 The relationship between air quality and public health is well-documented, with $PM_{2.5}$ exposure directly linked to increased mortality and cardiorespiratory disease (Anderson et al., 2012; World Health Organization, 2021). The global burden of these health impacts is highest in low-income countries (Ambient (outdoor) air pollution, 2026; Household air pollution, 2026). For a low-income country like Ethiopia, this problem is two-fold: outdoor air pollution related to open waste burning and relatively older vehicles, and indoor air pollution related to use of biomass fuels (which also contributes to outdoor air pollution).

35 Addressing $PM_{2.5}$ exposure is further hindered by resource limitations, leading to a lack of monitoring infrastructure. As air pollution varies across both space and time, high-resolution monitoring networks are needed for identifying pollution peaks and pinpointing human exposure (Karagulian, 2023; Li et al., 2020; Maji et al., 2017; Mushtaq et al., 2024). The reference method for $PM_{2.5}$ monitoring (gravimetry), and reference equivalent monitors are expensive regarding labour and material costs, hence generally not a feasible solution for low-income countries. In recent years, however, low-cost sensors (LCS) are

40 gaining traction as a viable alternative to traditional regulatory sites (Karagulian et al., 2019; Kumar et al., 2015; Suriano and Prato, 2023). Their low investment and maintenance costs make it feasible to set up dense networks (Kumar et al., 2015; Morawska et al., 2018). LCS are commonly sold as pre-assembled systems, but additional cost reduction is achieved by sourcing sensors from original equipment manufacturers (OEMs) for local assembly.

Light-scattering LCS introduce inherent data quality uncertainties regarding precision (consistency between identical units)

45 and accuracy (proximity to ‘the truth’). The relationship between light scattering and mass concentration to particle composition and shape varies across particle types. The *accuracy* of a sensor, without changing scatter to mass translation, might be good under one condition, while underperforming under another. This necessitates local validation under site-specific conditions rather than relying only on factory calibrations (Karagulian et al., 2019). Furthermore, sensor quality affects both the *precision* and *accuracy*, which varies from sensor type to sensor type. It is therefore important to validate specific sensor

50 types, rather than to let one low-cost sensor type stand as representative of others. A specific metric of sensor quality is its performance under high particulate loads, often used as a proxy for long-term stability (Tryner et al., 2020). This is particularly relevant in the Ethiopian context, where indoor environments frequently reach high concentrations (Admasie et al., 2019; Dingemane and Tademe, 2023; Tamire et al., 2021). Finally, humidity affects the accuracy of the scatter-to-mass translation. Increased relative humidity can lead to scattering enhancement (Zieger et al., 2013) due to hygroscopic particle growth and

55 changed optical properties (Liu et al., 2019). The κ -Köhler theory can be used to make a physical correction for the effect of hygroscopic particle growth when particle composition is constrained (Malings et al., 2020; Tryner et al., 2020). Others make non-physical correction with RH as variable within regression analyses (Malings et al., 2020; Zusman et al., 2020).

Among OEM sensors, the Sensirion SPS30 has become popular (Wesseling et al., 2024) and is frequently selected for its precision, accuracy and durability (Gabriel and Auer, 2023; Mahajan, 2022; Mujan et al., 2021; Park et al., 2021a, b; Riediker,

60 2022). Comparative studies often rank the SPS30 above others in terms of accuracy and precision (Sousan et al., 2021; Tryner et al., 2020). The reaction to RH is less than some other sensors (Hassani et al., 2023; Hong et al., 2021; Tryner et al., 2020).



The SPS30 is MCERTS certified for indicative ambient PM_{2.5} monitoring at concentrations below 75 µg m⁻³ (CSA Group Testing UK Ltd, 2025a) and was the first OEM LCS evaluated in Ethiopia (Dingemans and Tademe, 2023). Sensirion also offers another sensor, SEN55, which according to the company has the same specifications regarding PM sampling. Next to PM sampling, it has integrated temperature, humidity, VOC and NO_x measurements. The SEN55 is not MCERTS certified for PM_{2.5} measurements. While recent studies have begun testing the SEN55 and its variants (e.g., the SEN54) (Baguio et al., 2025; Rabuan et al., 2023; Rodríguez Rama et al., 2024; Wang et al., 2025), there remains a critical research gap: none of these studies compared the SEN55 against reference-equivalent instrumentation. Moreover, the SEN55 performance has not yet been tested under the specific indoor and outdoor environmental conditions characteristic of low-income countries like Ethiopia. Therefore, the objective of this study is to evaluate the performance and inter-model consistency of Sensirion SPS30 and SEN55 sensors through collocated gravimetric measurements in a representative Ethiopian urban environment. By presenting data from a long-term outdoor and intensive indoor campaign in Arba Minch, Ethiopia, we specifically aim to validate these sensors across a wide range of real-world conditions – from low-concentration backgrounds to extreme particulate loads (> 1000 µg m⁻³) characteristic of biomass-burning events. Our evaluation is structured across four key performance dimensions: (1) sensor precision and inter-unit consistency, (2) accuracy against gravimetric measurements, (3) sensor stability and digital truncation during high-concentration events, and (4) the influence of relative humidity on sensor performance.

2 Methods

2.1 Measurement locations

We conducted measurements in Arba Minch, a city in the South Regional State of Ethiopia. 70 % of annual rainfall is during two seasonal rainfall periods: September–November and March–May (Shalish et al., 2022). Temperatures range between 15.1 and 31.2 °C, at an average of 22.4 °C (Mekonnen, 2024). Based on the latest census and projections Arba Minch is with 200 000–300 000 residents the 14th most populated city of Ethiopia (Central Statistics Agency (Ethiopia), 2013, 2023).

Data has been collected in three phases: sensors and gravimetry in outdoor air (phase 1; December 2024–May 2025), sensors and gravimetry in indoor air with expected high concentrations (phase 2; June 2025), and sensors only in a residence (phase 3; July–September 2025). Photos of the locations are shown in Appendix A. During phase 1, measurements were conducted at two locations: close to the main entrance of the Arba Minch University campus (Outdoor 1), and inside a lab on the same campus behind an open window (Outdoor 2). Since concentration patterns and magnitudes of Outdoor 1 and Outdoor 2 were similar, we categorized both locations as representative for outdoor air on the campus (see Appendix A.2). PM_{2.5} sources are a mixture of background concentrations, traffic passing the campus and open waste burning of leaf and plant litter. During phase 2, measurements were conducted inside two campus kitchens (Kitchen 1 and 2). These locations were selected due to their use of biomass for cooking, with expected high PM_{2.5} concentrations. During phase 3, measurements were conducted



behind an open window inside a residence on campus (Residence). During daytime, concentrations were like campus (Outdoor 1 and 2) concentrations, while in the evenings nearby residential sources resulted in higher concentrations.

95 For comparison with phase 2, Appendix G presents a reanalysis of biomass cooking measurements from other kitchens (Dingemanse and Tademe, 2023). Additionally, to substantiate the systematic nature of our results across diverse climates, Appendix H provides data from four months of background measurements in Hyltemossa, Sweden. At this location, three SPS30 and one SEN55 were collocated with a Palas Fidas (reference equivalent monitor). This supplementary dataset allows for an evaluation of the SEN55-to-SPS30 relationship and the impact of relative humidity under environmental conditions
100 distinct from those in Arba Minch.

2.2 Instruments

2.2.1 Low-cost sensors

The Sensirion SPS30 is a sensor based on light-scattering (wavelength 660 nm), with one inlet for sample flow and one inlet for filtered sheath air (Fig. A1). Air is drawn into the sensor, where it passes a laser beam and photodiode. Particles in the
105 airstream cause light scattering, which is detected by the photodiode. The detected scatter is used as measurement of mass and number concentrations. The SPS30 reports number concentrations in five bins (upper bin borders of 0.5, 1, 2.5, 4 and 10 μm) and mass concentrations in four particle sizes (PM_1 , $\text{PM}_{2.5}$, PM_4 , PM_{10}). As per company specifications, the $\text{PM}_{2.5}$ measurement range is 0–1000 $\mu\text{g m}^{-3}$, with an uncertainty of $5 \mu\text{g m}^{-3} + 5 \% < 100 \mu\text{g m}^{-3}$, and 10 % at 100–1000 $\mu\text{g m}^{-3}$ (Sensirion, 2023). The sensor can however report much higher values, well over 50 000 $\mu\text{g m}^{-3}$ (Dingemanse, 2022).

110 The Sensirion SEN55 uses the same measurement technology for PM (light-scatter) and reports the number and mass concentration in the same size bins. Like the SPS30, it has one sample flow inlet and one filtered inlet (Fig. A1). Its measurement range and uncertainty as per company specifications is the same as the SPS30 (Sensirion, 2022). The theoretical maximum value it can report is 6553.4 $\mu\text{g m}^{-3}$, as all output is truncated to a 16-bit unsigned integer with one digit. Apart from the dimensions and the output truncation, the main difference with the SPS30 is that the SEN55 has additional integrated
115 sensor modules for temperature, relative humidity, VOC and NO_x .

Both the SPS30 and SEN55 $\text{PM}_{2.5}$ mass concentrations are factory calibrated to a TSI DustTrak DRX 8533. The SPS30 $\text{PM}_{2.5}$ number concentrations are calibrated to a TSI OPS 3330 (Sensirion, 2022, 2023). Calibration is conducted with potassium chloride (Sensirion, 2020).

2.2.2 Reference instruments

120 For outdoor measurements, filter samples were collected with a Leckel Low Volume Sampler (LVS6-RV; LVS) equipped with a $\text{PM}_{2.5}$ inlet. The LVS has a continuous flow rate of $2.3 \text{ m}^3 \text{ hr}^{-1}$, with which it loads a 47 mm filter. The LVS6-RV is a standard reference sampler according to specifications in CEN EN 12341. In case of power interruption, upon restart of power



the LVS automatically continue until the preset sampling time is reached. We tracked moments of power interruption with a power logger.

125 For indoor measurements, two UPAS V2.0 instruments with PM_{2.5} inlet were used. The UPAS has a flow rate of 1 L min⁻¹, with which it loads a 37mm filter.

The flow rates were validated during the measurement period with a handheld Kytola flow meter (models A-8PR and A-2BR for the LVS and UPAS, respectively). After the measurement period, the flow rates were validated with the TSI Flow Calibrator (model 4048). The LVS and UPAS flow rates were within 5 % of their expected flow rate.

130 Gravimetric analysis of filters was conducted with a Mettler Toledo AE240, which has a repeatability of 20 µg (Appendix B.1). We estimated the LVS and UPAS expanded uncertainty (95 % confidence interval) to be respectively 6.0 and 12.2 % (Appendix B.4).

2.2.3 Relative humidity and temperature measurements

We measured relative humidity (RH) and temperature (T) with the SEN55, which has rated accuracies of ± 4.5 % and 0.45 °C for RH and T, respectively (Sensirion, 2022). To verify these accuracies, we compared the SEN55 data to a collocated thermohygrograph (THG), finding high correlations ≥ 0.96 (Appendix C.1.1). The SEN55 exhibited a temperature offset that propagated into an RH offset. Since this offset is likely due to self-heating (Appendix C.1.3), we assumed that the SEN55 RH and T are the best indication of the corresponding PM measurements.

2.3 Measurements

140 Across three boxes, six SPS30 (SPS1-6) and six SEN55 (SEN1-6) were used throughout the study. For data logging, the SPS30 and SEN55 sensors were interfaced with a microprocessor, a memory card module, and a clock module (Appendix A.1). We placed the sensor systems at a height of 1 to 2.2 meters (details in Appendix A.2). Table 1 gives an overview of all measurement times.

Table 1: Sensor installation periods and number of gravimetric samples.

Period	Location	Sensors	Sensor measurement days	Gravimetry samples
Phase 1	Outdoor 1	Box 1 (SPS1-3, SEN1)	09-01-2025–29-01-2025	7
			27-03-2025–16-05-2025	11
Phase 1	Outdoor 2	Box 1 (SPS1-3, SEN1)	31-12-2024–09-01-2025	5
			29-01-2025–17-03-2025	31
Phase 2	Kitchen 1	Box 2 (SPS4-6, SEN2-3, SEN6)	09-06-2025–24-06-2025	12
Phase 2	Kitchen 2	Box 1 (SPS1-3, SEN1)	10-06-2025–28-06-2025	18
Phase 2	Kitchen 2	Box 3 (SEN4-5)	09-06-2025–28-06-2025	
Phase 2	Kitchen 2	Box 2 (SPS4-6, SEN2-3, SEN6)	24-06-2025–28-06-2025	
Phase 3	Residence	Box 2, Box 3 (SPS4-6, SEN2-6)	10-07-2025–19-09-2025	0

145 For phase 1 and phase 3, measurement frequency of all sensors was set to 1 minute. For phase 2, measurement frequency was set to 10 seconds. Details regarding sensor data management are provided in Appendix A.3. Details of gravimetric procedures



and an overview of all gravimetric measurements are provided in Appendix B. We discarded eight filter samples (9 % of 85 samples, see Appendix B.3).

2.4 Data analysis

150 We first converted raw sensor into ten-minute averages. Depending on the metric (see Sections 2.4.1 and 2.4.2), we then used hourly or daily averages for quality evaluation. We included only hour-averages of hours that had a full set of six ten-minute averages, while we included daily averages of days that contained at least 18 hour-averages.

2.4.1 Precision

For comparison of identical sensors (*precision*), we use the coefficient of variation (CV), also called relative standard deviation
155 (Tryner et al., 2020). We calculated the CV with Eq (1) (Sousan et al., 2016):

$$CV = \frac{1}{n} \sum \frac{\sigma_i}{\mu_i} \quad (1)$$

Where, σ_i is the standard deviation and μ_i is the mean of measurements of identical sensors during time period i , and n is the number of time periods. The duration of the time period is not prescribed. We use hourly averages since that is a common reporting period for air quality monitors. According to EPA and NIOSH, CV values below 10 % are acceptable (EPA, 2006;
160 NIOSH, 2012).

We additionally use the between-sampler uncertainty (u_{bs}) as defined in the Guide for Demonstration of Equivalence (GDE) (European Commission, 2010). The u_{bs} must be calculated with Eq (2) (European Commission, 2010):

$$u_{bs} = \sqrt{\frac{\sum (y_{i,1} - y_{i,2})^2}{2n}} \quad (2)$$

Where, $y_{i,1}$ and $y_{i,2}$ are the results of parallel measurements for time period i , and n is the number of time periods. Time period
165 length should be 24 hours. The GDE prescribes to test the u_{bs} for all data points, as well as for datasets of all values below and above $18 \mu\text{g m}^{-3}$ separately. There are acceptable u_{bs} values at two levels: $< 2.5 \mu\text{g m}^{-3}$ for fixed reference-grade measurements (European Commission, 2010), and $< 5 \mu\text{g m}^{-3}$ for indicative sampling (CSA Group Testing UK Ltd, 2025a). The u_{bs} is an absolute value, meant for outdoor concentration measurements. With equal relative errors, high concentrations likely lead to absolute errors beyond 2.5 and $5 \mu\text{g m}^{-3}$. For the calculation of the u_{bs} we therefore ignored any hours with ten-minute averages
170 beyond $1000 \mu\text{g m}^{-3}$.

2.4.2 Accuracy

For comparison of sensors with gravimetry measurements, we calculated Pearson's correlation (r), root mean square error (RMSE) and slope (S) and coefficient of determination (R^2) from a linear regression model of slope only ($y = S * x$), with gravimetric measurements as y and sensor measurements as x . As linear model, we used weighted least squares (WLS)



175 regression. The regression is weighted with $\frac{1}{y_i^2}$ to give data points at low concentration values equal weight with those of high concentration values. Under appendix D.2, we show results of WLS of a model including intercept I ($y = S * x + I$). We also used accuracy metrics published by the National Institute for Occupational Safety and Health (NIOSH): accuracy error (AE) with accompanying bias (B). We calculated B with Eq. (3) (NIOSH, 2012):

$$B = \frac{1}{n} \sum \left(\frac{x_i}{y_i} - 1 \right) \quad (3)$$

180 Where, x_i is the concentration of the sensor and y_i the concentration of the reference instrument for time period i , and n is the number of time periods. When B is larger than |10 %|, corrected data x_{new} must be calculated based on old data x_{old} with Eq. (4) (NIOSH, 2012):

$$x_{new} = \frac{x_{old}}{B + 1} \quad (4)$$

The AE is the maximum difference between $\frac{x_i}{y_i}$, as percentage of y_i , at a 0.95 probability (NIOSH, 2012). We calculated the

185 AE as the upper value of the confidence interval at 90% of all values $\frac{x_i}{y_i}$. Acceptable values for AE are < 25 % (NIOSH, 2012).

For outdoor conditions, we additionally use the expanded uncertainty (W_{CM}) as defined in the GDE. The W_{CM} should be tested both for the whole dataset, as well as a dataset of values > 18 $\mu\text{g m}^{-3}$. For the W_{CM} , a linear relationship between sensor and reference measurements is assumed. For this linear relationship, algorithms of orthogonal regression (OR) should be used. If slopes are significantly different from 1, and/or the intercept is significantly different from 0, data should be corrected for this.

190 We conducted regression calculations and determinations of slope and intercept significance according to the equations shown in the GDE (GDE section 9.5 and GDE Appendix B). Part of these calculations include a correction for the uncertainty of the reference method. We used 0.9 $\mu\text{g m}^{-3}$ for this (see Appendix B.4). There are acceptable W_{CM} values at two levels: for fixed reference-grade measurements < 25 %, while for indicative sampling < 50 % (European Union, 2015).

2.4.3 High-concentration evaluation

195 We investigated how high particle loads affect sensor operation by checking precision during low-concentration hours (average < 50 $\mu\text{g m}^{-3}$), within one or two hours after an hour that contained a high concentration measurement (> 1000 $\mu\text{g m}^{-3}$).

We also tested the validity of data at the SEN55's digital truncation limit (6553.4 $\mu\text{g m}^{-3}$, see section 2.2.1). A Pearson Chi-square test was performed on two SEN55/SPS30 pairs to see if the maximum value occurrences matched significantly at both 10-minute and hourly resolutions. To measure the impact of truncation, we compared the SEN55 to SPS30 correlation slopes
200 of the complete dataset against a version excluding these maximum values. Finally, we compared five data handling strategies for high concentrations: (1) the full, untruncated dataset, (2) values > 6553.4 $\mu\text{g m}^{-3}$ truncated to that value (SEN55 logic), (3) values > 6553.4 $\mu\text{g m}^{-3}$ removed as errors, (4) data points beyond 1000 $\mu\text{g m}^{-3}$ truncated to 1000 $\mu\text{g m}^{-3}$ (manufacturer specification interpretation), or (5) values > 1000 $\mu\text{g m}^{-3}$ removed.



2.4.4 Effect of relative humidity

205 To check whether the SEN55 and SPS30 are affected similarly by relative humidity, we evaluated the SEN55 to SPS30 ratio across relative humidity levels.

To check for a possible hygroscopic effect, we evaluated the SEN55 to gravimetry ratio for different relative humidity bins. We did this for both the original SEN55 data, as well as SEN55 data corrected for a theoretical hygroscopic growth. We used the κ -Köhler theory to calculate the theoretical growth factor of the mass based on the relative humidity GF(RH), with

210 Eq. (5) (Blaga, 2024; Crilley et al., 2018; Petters and Kreidenweis, 2007):

$$GF(RH) = 1 + \kappa * \frac{RH}{\frac{\rho_{particle}}{\rho_{water}} * (100 - RH)} \quad (5)$$

The density of water ρ_{water} is 1 g cm^{-3} , and we used 1.65 g cm^{-3} as bulk dry particle density $\rho_{particle}$ (Crilley et al., 2018). κ is a constant representing the hygroscopicity of the particles. There is high variation in hygroscopicity per particle (and the related complexity in one κ -value for particle mixtures). We could also find no studies on hygroscopicity of the Ethiopian urban and rural environment. We therefore use a κ -value suggested for continental aerosols in general: 0.3 (Andreae and Rosenfeld, 2008).

215

We only evaluate relative humidity effects for phase 1 and 3 data. The phase 2 measurements had a low relative humidity variation (40–60 %) with extreme concentration events, hence biasing the analysis at a limited range of relative humidity.

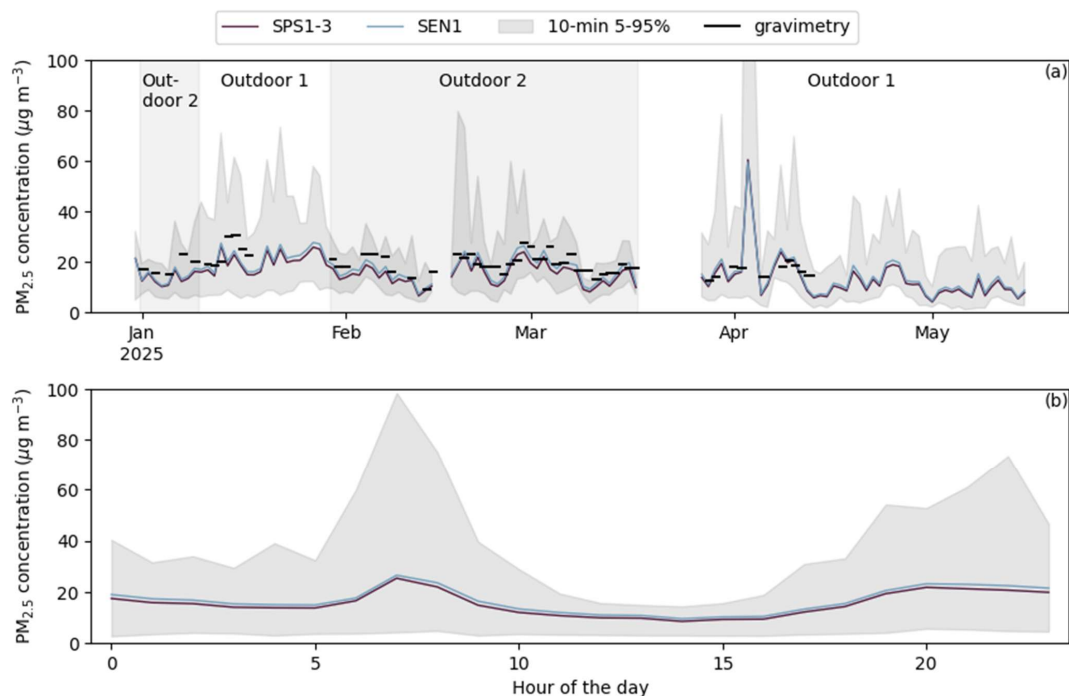
3. Results

220 3.1 Concentration levels

This section shows the conditions of our measurements. We present the concentration levels measured in the three phases (3.1.1 – 3.1.3), as well as the temperature and relative humidity during the measurement period (3.1.4).

3.1.1 Phase 1 measurements

Figure 1 shows the concentrations measured at locations Outdoor 1 and 2.



225

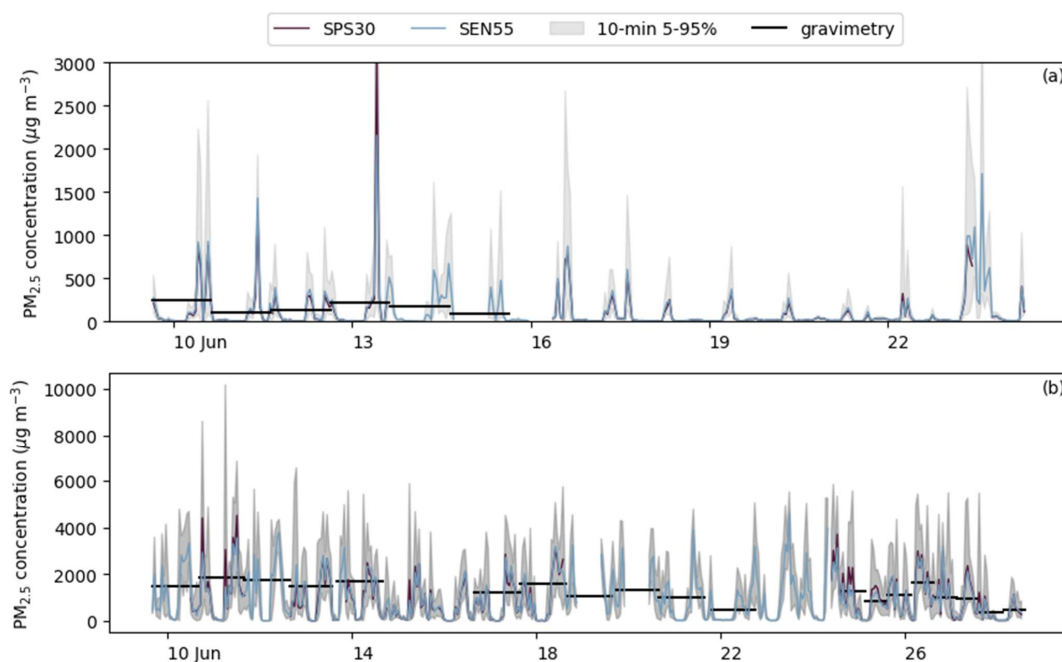
Figure 1: gravimetry measurements, sensor daily averages (a) and sensor averages per hour of the day (b), as well as 5–95 % of 10-minute averages, at locations Outdoor 1 and 2. Concentrations in panel (b) are from all days across both locations.

Daily averages at lab and gate on average were $14.8 \mu\text{g m}^{-3}$ (min–max 4–33 $\mu\text{g m}^{-3}$). Ten-minute averaged concentrations reached over $80 \mu\text{g m}^{-3}$. There is a diurnal pattern with elevated concentrations in the morning (6:00–9:00) and evening (18:00–

230 22:00). The morning and evening peaks result from traffic and cooking activities.

3.1.2 Phase 2 measurements

Figure 2 shows concentrations measured in the two kitchens.



235 **Figure 2: PM_{2.5} gravimetric measurements, hourly averages and 5-95% 10-minute averages at Kitchen 1 (a) and Kitchen 2 (b). The top panel y-scale is limited to 3000 µg/m³ for visibility; only on June 13 the 95 % of 10-minute averages was beyond 3000 µg m⁻³ (up to 10 000 µg m⁻³).**

Concentrations at both kitchens were significantly higher than outdoor concentrations. At Kitchen 1, hourly averages regularly reached up to 1000 µg m⁻³, while at Kitchen 2 they regularly reached up to 4000 µg m⁻³. The gravimetric measurements are an indication of longer-term averages: 100–400 µg m⁻³ at Kitchen 1 and 500–2000 µg m⁻³ at Kitchen 2.

240 3.1.3 Phase 3 measurements

Figure 3 shows the concentrations measured at location Residence.

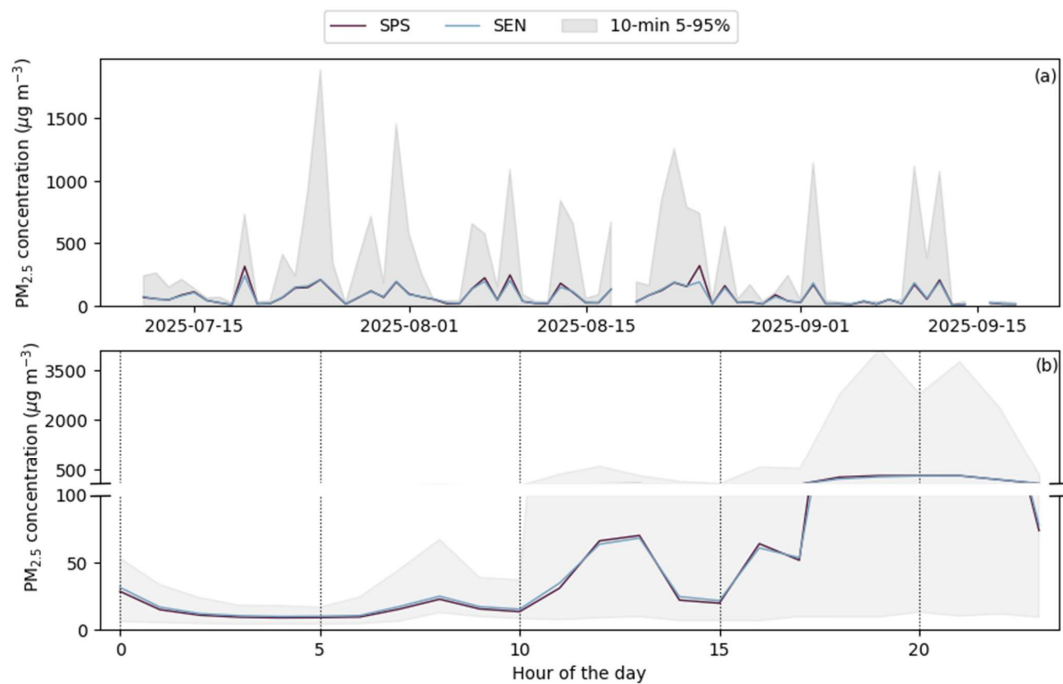


Figure 3: PM_{2.5} daily averages (a) and averages per hour of the day (b), as well as 5–95 % of 10-minute averages, at location Residence. Panel (b) shows the same data in two linear scales: 0–100 and 100–4000 µg m⁻³.

245 At location Residence, daily averages were in some cases higher than 200 µg m⁻³. Between 2:00 and 10:00, concentrations at this location were comparable to those at Outdoor 1 and 2. However, in the afternoon and even more in the evening high concentrations were measured. Ten-minute averaged concentrations ranged up to 4000 µg m⁻³ between 18:00 and 22:00.

3.1.4 Temperature and relative humidity

250 Daily average temperatures (T) ranged from 20 to 32 °C. Relative humidities (RH) were lower in January–March, while hourly relative humidities regularly were > 80 % in March–May. T and RH conditions during precision measurements were representative for normal conditions of Arba Minch, while relative humidities during accuracy measurements were on average lower (Appendix C.2).



3.2 Precision

In the following sections, we evaluate the precision of the sensors through the between-sampler uncertainty u_{bs} (3.2.1), the coefficient of variation (3.2.2), and the possibility of improving the accuracy through sensor-specific corrections (3.2.3).

3.2.1 Between-sampler uncertainty

Table 2 shows the between-sampler uncertainty u_{bs} , Eq. (2), based on daily averages with at least 18 hours of data, for all SPS30 and SEN55 sensor pairs, as well as two SPS30 to SEN55 pairs.

Table 2: u_{bs} for collocated sensor pairs across the study locations. We calculated the u_{bs} based on all 24-hour averages, and separately on those below and those above $18 \mu\text{g m}^{-3}$ $\text{PM}_{2.5}$ (see section 2.4.1).

Sensor 1	Sensor 2	All		$\leq 18 \mu\text{g/m}^3 \text{PM}_{2.5}$		$> 18 \mu\text{g/m}^3 \text{PM}_{2.5}$	
		N	u_{bs} ($\mu\text{g m}^{-3}$)	N	u_{bs} ($\mu\text{g m}^{-3}$)	N	u_{bs} ($\mu\text{g m}^{-3}$)
SPS1	SPS2	104	0.46	72	0.32	32	0.68
SPS1	SPS3	104	0.44	71	0.37	33	0.57
SPS2	SPS3	104	0.23	71	0.16	33	0.32
SPS4	SPS5	75	1.2	22	0.64	53	1.31
SPS4	SPS6	74	1.4	22	0.74	52	1.6
SPS5	SPS6	74	0.44	22	0.13	52	0.52
SEN2	SEN3	66	1.3	17	0.57	49	1.5
SEN4	SEN5	63	1.5	19	0.69	44	1.7
<i>SPS30 to SEN55 pairs^a</i>							
SPS1	SEN1	104	1.2	61	1.0	43	1.4
SPS6	SEN6	74	2.7	16	1.1	58	3.0

a: For comparing SEN55 to SPS30 sensors, we selected two SEN55 sensors that were installed in systems together with SPS30 sensors (see appendix A.2).

For both the SPS30 and the SEN55, all u_{bs} values are lower than the GDE requirement of $2.5 \mu\text{g m}^{-3}$ for fixed reference-grade measurements. This is the case for both datasets of values below and above $18 \mu\text{g m}^{-3}$. At higher concentrations, with a similar relative error, the error becomes bigger, hence in all cases the u_{bs} is higher for the datasets with higher concentrations.

The difference between SPS30 and SEN55 instruments is larger than between identical sensor types. Comparing SPS30 to SEN55 pairs results in between-sampler uncertainties of $1.0\text{--}3.0 \mu\text{g m}^{-3}$. This is below the MCERTS threshold for indicative sensors ($5 \mu\text{g m}^{-3}$), but not below that of $2.5 \mu\text{g m}^{-3}$ for fix reference-grade measurements (GDE). This is especially due to measurements under higher concentrations: the highest u_{bs} is $3 \mu\text{g m}^{-3}$, while that of lower values is $1.14 \mu\text{g m}^{-3}$. Also, the SPS6 to SEN6 comparison results in higher u_{bs} values than those for SPS1 to SEN1, because we used SPS6 and SEN6 only during the high-concentration phases (2 and 3).

3.2.2 Coefficient of variation

Table 3 shows the CV, Eq. (1), based on 1-hour averaged data, for all SPS30 and SEN55 sensor pairs and two SPS30 to SEN55 pairs, for both the whole dataset as well as three concentration ranges.

Table 3: Number of data points (N) and CV for collocated sensor pairs across the study locations. The CV is calculated based on all hour-averages, and separately for the ranges $0\text{--}100$, $100\text{--}1000$ and $> 1000 \mu\text{g m}^{-3}$.



Sensor 1	Sensor 2	All data		$\leq 100 \mu\text{g m}^{-3}$		100–1000 $\mu\text{g m}^{-3}$		$> 1000 \mu\text{g m}^{-3}$	
		N	CV (%)	N	CV (%)	N	CV (%)	N	CV (%)
SPS1	SPS2	2695	2.4	2689	2.4	6	4.4	0	-
SPS1	SPS3	2695	2.9	2689	2.9	6	2.7	0	-
SPS2	SPS3	2943	1.4	2748	1.3	102	2.4	93	2.5
SPS4	SPS5	2014	4.7	1718	4.4	217	5.5	79	7.7
SPS4	SPS6	2014	4.9	1716	4.7	219	6.2	79	5.5
SPS5	SPS6	2014	1.4	1716	1.1	218	2.5	80	3.1
SEN2	SEN3	1776	5.1	1549	4.8	173	7.5	54	3.9
SEN4	SEN5	1922	4.2	1494	3.8	250	6.6	178	3.8
SPS30 to SEN55 pairs ^a									
SPS1	SEN1	2695	8.4	2689	8.4	6	1.9	0	-
SPS6	SEN6	2014	8.7	1703	8.7	228	8.3	83	8.7

a: For comparing SEN55 to SPS30 sensors, we selected two SEN55 sensors that were installed in systems together with SPS30 sensors (see appendix A.2).

For all SPS30 and SEN55 sensor pairs, the CV is lower than the threshold for acceptable values set by EPA and NIOSH (10 %). This holds for datasets of all concentration levels, including those beyond the range specified by the manufacturer ($> 1000 \mu\text{g m}^{-3}$). It also holds for SPS30 to SEN55 pairs.

280 3.2.3 Reducing variation

While the precision results of both the SPS30 and the SEN55 are below GDE, NIOSH and EPA thresholds, we can see whether the values can be lowered by distinguishing between random and continuous variations between sensor pairs. Table 4 shows the mean sensor 1 to sensor 2 ratio, and the u_{bs} and CV after correcting for this ratio.

285 **Table 4: Average ratios (sensor 1 / sensor 2), and u_{bs} and CV for collocated sensor pairs across the study locations after correcting for the average ratios.**

Sensor 1	Sensor 2	Average ratio ^a	u_{bs} corrected all data ($\mu\text{g m}^{-3}$)	u_{bs} corrected > 18 $\mu\text{g m}^{-3}$ ($\mu\text{g m}^{-3}$)	CV corrected All data (%)	CV corrected > 1000 $\mu\text{g m}^{-3}$ (%)
SPS1	SPS2	0.97	0.3	0.5	2.0	-
SPS1	SPS3	0.96	0.3	0.3	1.7	-
SPS2	SPS3	0.99	0.2	0.4	1.3	2.1
SPS4	SPS5	0.94	0.5	0.6	1.2	3.4
SPS4	SPS6	0.94	0.6	0.7	1.6	2.4
SPS5	SPS6	1.00	0.4	0.5	1.4	3.2
SEN2	SEN3	1.05	1.0	1.1	2.8	5.3
SEN4	SEN5	0.96	1.1	1.3	2.4	3.3
SPS30 to SEN55 pairs ^b						
SPS1	SEN1	0.89	0.6	1.0	2.6	-
SPS6	SEN6	0.90	1.1	1.3	3.1	9.3

a: The average ratio is calculated based on ten random selections by NumPy's random number generator of 30 % of the data.

b: For comparing SEN55 to SPS30 sensors, we selected two SEN55 sensors that were installed in systems together with SPS30 sensors (see appendix A.2).



After correcting for the average ratios, the u_{bs} and CV are in most cases reduced. Part of the difference between individual pairs is not random, but with a continuous direction. This implies that the accuracy of individual sensors can be improved if users can collocate them to establish individual sensor corrections.

For the SPS30 to SEN55 the average ratio is lower than the ratios between identical sensors (0.89–0.9, while 0.96–1.05 for identical sensors). The correction therefore has a larger effect. For uncorrected values we saw clearly higher CV and u_{bs} values for SPS30 to SEN55, but with correction they are in the same range as those of identical sensor type pairings. There is one notable exception: the correction does not lead to a decrease of the CV under $> 1000 \mu\text{g m}^{-3}$ averages (9.3 % after correction versus 8.7 % before correction. In section 3.4 we will show that a separate high-concentration effect nulls the SEN55 to SPS30 ratio that is otherwise observed.

3.3 Accuracy

We present results on the sensor accuracies in comparison with gravimetric measurements subsequently for outdoor measurements (3.3.1) and indoor measurements (3.3.2).

3.3.1 Outdoor concentration levels

We show scatter plots of sensor versus gravimetry $\text{PM}_{2.5}$ outdoor concentrations in Fig. D2. Table 5 shows all quality metrics for comparison of sensor average values with filter measurements of the LVS under outdoor concentration levels.

Table 5: Quality metrics under outdoor conditions for $\text{PM}_{2.5}$ sensor measurements (per ID) in comparison to gravimetric measurements: number of pairings (N), Pearson correlation (r), Weighted Least Squares (WLS) slope (S) with 95 % confidence interval (CI) and R^2 , root mean square error (RMSE, before→after correction for S), bias (B) and AE before→after correction for B, orthogonal regression (OR) significant correction (sign. corr.) and expanded uncertainty (W_{CM}) before→after this correction.

ID	N	r	WLS ^a		RMSE ($\mu\text{g m}^{-3}$)	B (%)	AE (%)	OR, all data		OR, $>18 \mu\text{g m}^{-3}$		
			S [CI] (R^2)					Sign.	W_{CM} (%)	N	Sign.	W_{CM} (%)
SPS1	53	0.90	1.23 [1.19–1.26] (0.99)		4.2→2.1	-19	22→10	1.23	38→10	41	1.22	48→12
SPS2	53	0.88	1.20 [1.16–1.24] (0.99)		4.0→2.3	-18	21→11	1.21	36→12	41	1.21	44→15
SPS3	53	0.89	1.19 [1.15–1.23] (0.99)		3.8→2.2	-17	20→11	1.20	33→12	41	1.19	42→14
SEN1	53	0.90	1.11 [1.08–1.14] (0.99)		2.9→2.1	-11	15→10	1.12	21→12	41	1.11	31→14

a: For WLS, a model with slope only is shown here. Under Appendix D.2 we show results for a linear model with intercept.

b: For calculation of the W_{CM} , correction for slopes significantly different from one and/or intercepts significantly different from zero is required (see section 2.4.2). In all cases, there were significant slopes only.

All sensors require a positive correction as they all reported lower values than the gravimetric measurements. The SPS30 sensors have slopes between 1.19 and 1.23 (significantly different from 1), while the SEN55 has a slope of 1.11 (significantly different from 1). After correction, the accuracy errors and expanded uncertainties are all lower than the NIOSH and GDE thresholds of 25 % (10–12 %). The W_{CM} for all concentrations beyond $18 \mu\text{g m}^{-3}$ is in the same order of magnitude: between 12 and 15 %. The 95 % confidence interval of the SEN55 slope reaches up to 1.14, while those of the SPS30 slopes start from 1.15. The slopes are significantly different from each other; the SEN55 is measuring significantly higher than the SPS30. This



corresponds with the finding under section 3.2 that a direct SPS30 to SEN55 comparison revealed bigger differences than those amongst identical sensor types.

When we apply the average correction factor for the SPS30 (1.21) to the SEN55 data, direct comparison with gravimetry results in an RMSE of $2.7 \mu\text{g m}^{-3}$, an AE of 12.7 %, and a W_{CM} of 23 %. While the values increase in comparison to correction for the SEN55-slope, the accuracy errors are still within the range of reference equivalent instruments (< 25 %). If one can locally calibrate a SEN55, this is preferred. However, the SPS30 and SEN55 are *similar enough* to allow for extrapolating data quality results of the SPS30 to the SEN55.

3.3.2 Indoor concentration levels

We show scatter plots of sensor versus gravimetry $\text{PM}_{2.5}$ concentrations in Fig. D3. Table 6 shows all quality metrics for comparison of sensor average values with filter measurements of the UPAS under indoor high-concentration levels.

Table 6: Quality metrics under indoor conditions for sensors (ID) in comparison to gravimetric measurements: number of pairings (N), Pearson correlation (r), Weighted Least Squares (WLS) slope (S) with 95 % confidence interval (CI) and R^2 , root mean square error (RMSE, before→after correction for S), bias (B) and AE before→after correction for B

Sensor	N	r	WLS ^a S [CI] (R^2)	RMSE ($\mu\text{g m}^{-3}$)	B (%)	AE (%)
SEN3	10	0.94	1.11 [0.97–1.25] (0.97)	201→106	-12	23→19
SEN4	15	0.91	1.24 [1.11–1.36] (0.97)	301→195	-22	28→18
SEN5	14	0.94	1.25 [1.15–1.35] (0.98)	312→155	-21	26→13
SPS2	11	0.87	1.18 [1.02–1.35] (0.96)	363→254	-19	28→22
SPS3	11	0.89	1.16 [1.01–1.31] (0.97)	338→243	-16	26→21
SPS4	12	0.99	1.19 [1.09–1.29] (0.98)	147→78	-17	23→14
SPS5	12	0.99	1.07 [0.97–1.17] (0.98)	90→84	-8	17→16
SPS6	12	0.98	1.10 [1.00–1.20] (0.98)	115→95	-11	18→15
SEN6	12	0.99	1.01 [0.93–1.10] (0.98)	73→76	-2.9	14→14
All SPS30	58	0.94	1.14 [1.09–1.18] (0.97)	236→180	-14	19→16
All SEN55	51	0.93	1.15 [1.09–1.20] (0.97)	250→187	-15	21→16

a: For WLS, a model with slope only is shown here. Under Appendix D.2 we show results for a linear model with intercept.

For all sensors, after correction for an individual bias, the AE is lower than the NIOSH threshold of 25 %. The individual slopes, however, range from 1.07 to 1.19 (SPS30) and 1.01 to 1.25 (SEN55). The high, highly localized and highly variable concentration patterns under these circumstances are most likely one reason for these slope differences. SEN4 and SEN5 were on the same box (see Appendix A.1), and their slope is similar (1.24 to 1.25). This is the same for SPS2 and SPS3. This would suggest that under high concentrations from close-by sources, location and orientation of the sensors matters.

Slopes based on all SPS30 and SEN55 to gravimetry comparisons are the same: 1.14 and 1.15 with almost identical confidence intervals. When correcting data of all sensors with a slope of 1.14, accuracy errors for individual sensors range from 15 to 22 %. In other words: while individual correction factors result in higher data quality, the accuracy error with a same correction factor for all sensors (SPS30 and SEN55 alike) is still within the NIOSH range of acceptable values (< 25 %).



3.4 Sensor quality under high concentration conditions

340 We evaluate the precision after high concentration events (3.4.1), the effect of SEN55 digital truncation (3.4.2), and the effects
 of possible options for dealing with high concentration values (3.4.3).

3.4.1 Precision after high concentrations

Figure 4 shows, for collocated sensor pairs, all hourly averages of all hours one or two hours after an hour with a measurement
 beyond $1000 \mu\text{g m}^{-3}$. All datasets are split in half, chronologically, to evaluate whether there is an effect on the sensor precision

345 over time.

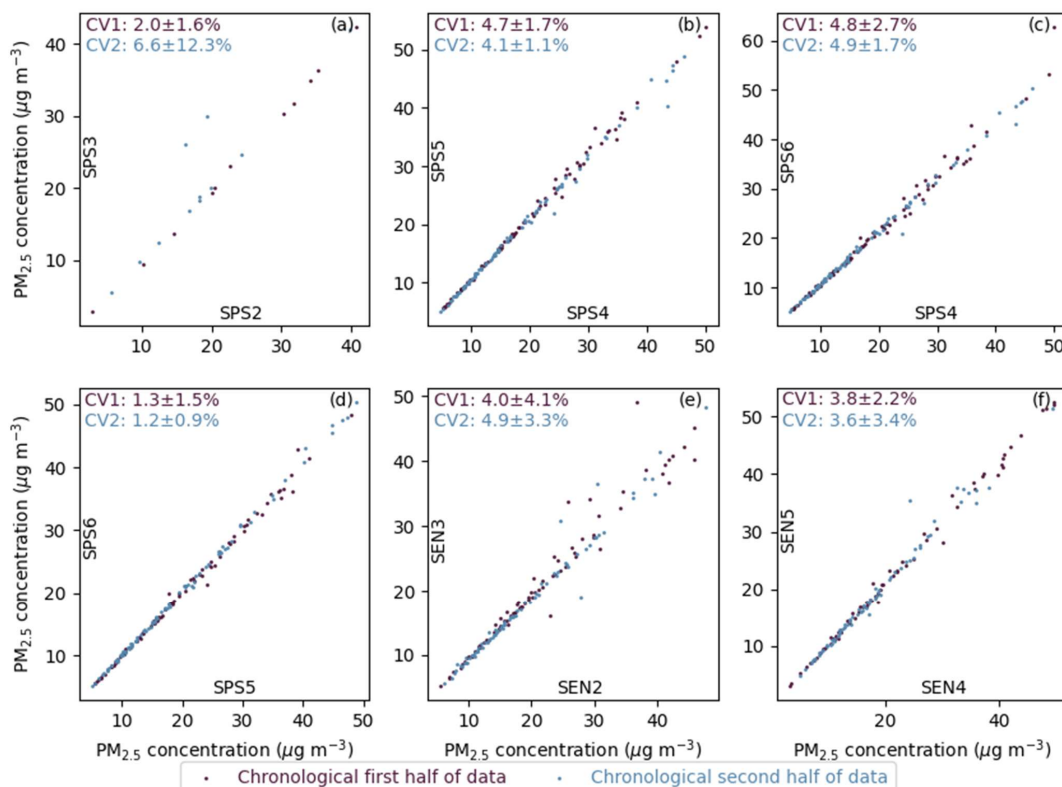


Figure 4: Hourly averages one or two hours after an hour with concentrations beyond $1000 \mu\text{g m}^{-3}$, split chronologically in two.



For all sensor pairs, the variation across them is below the EPA and NOISH threshold of 10 %. The CVs of the first and second half of the data do not differ significantly from each other. At location Residence, across two months of almost daily high-concentrations in the evening, eight sensors consistently returned to similar low readings under low-concentration conditions (Fig. E1). The precision of the sensor remains equally high, also after multiple high-concentration events.

3.4.2 Behavior at SEN55 digital truncation level

The SEN55 truncates all values beyond $6554.3 \mu\text{g m}^{-3}$ to that maximum value (see section 2.2.1), while the SPS30 reports higher values. A Pearson Chi-square test based on the hour- and 10-minute cutoff occurrences for two SPS30 to SEN55 sensor pairs (SPS4 to SEN3 and SPS6 to SEN6) resulted in all cases in a p-value $\ll 0.001$ (Appendix E.2). The SEN55 cutoff-values are significantly matched to SPS30 values beyond the cutoff.

The extent of this effect fully depends on the number and magnitude of such occurrences. Ordinary least squares regression on hourly averages between the two SPS30 and SEN55 pairs ($\text{SEN55} \cdot \text{slope} = \text{SPS30}$) resulted in slopes of 1.06 and 1.00 for all hourly averages. When ignoring the cutoff occurrences, the slopes become 0.92 and 0.93. For measurements below $6553.4 \mu\text{g m}^{-3}$, the SPS30 is measuring lower than the SEN55. Measurements beyond the cutoff, however, by definition result in higher values for the SPS30. Under indoor conditions, the higher SEN55 measurements are compensated by the cutoff effect. This is a likely explanation for our finding of similar slopes for SEN55 and SPS30 to gravimetry under indoor conditions (section 3.3.2).

The ratio of SPS30 to SEN55 of 0.92-0.93 for the above pairs' measurements below $6553.4 \mu\text{g m}^{-3}$ is similar to the ratio in slopes to gravimetry found under outdoor conditions (section 3.3.1; $1.11 / 1.21 = 0.92$). The above pairs' measurements are from phase 2 and 3, while the outdoor condition measurements are from phase 1. Also, the outdoor measurements come from other sensor units (SEN1 and SPS1-3 versus here SEN3,6 and SPS4,6). The SEN55 to SPS30 ratio is therefore found in three sensor pairs under two concentration regimes.

3.4.3 Options for dealing with high-concentration values

Data users and sensor system builders can make different choices in dealing with high-concentration values. We distinguish five situations: (1) using all data as is, (2) truncation to $6553.4 \mu\text{g m}^{-3}$, (3) removal of any value beyond $6553.4 \mu\text{g m}^{-3}$, (4) truncation to $1000 \mu\text{g m}^{-3}$, (5) removal of any value beyond $1000 \mu\text{g m}^{-3}$. Table 7 shows the bias and accuracy errors for sensors in comparison to gravimetry, for these five situations. Scatter plots are shown in Fig. E2.

Table 7: accuracy error (AE) and bias (B) based on all SPS30 and SEN55 to gravimetry data pairs under indoor conditions, for five situations of dealing with high $\text{PM}_{2.5}$ concentration values.

Situation	SPS30 sensors			SEN55 sensors		
	AE before correction %	Bias (B) %	AE after correction %	AE before correction %	Bias (B) %	AE after correction %
1 (All data)	19	-14	16			



2 ($\geq 6553.4 \mu\text{g m}^{-3}$ truncation)	24	-21	15	21	-15	16
3 ($\geq 6553.4 \mu\text{g m}^{-3}$ removal)	34	-31	18	31	-27	18
4 ($\geq 1000 \mu\text{g m}^{-3}$ truncation)	60	-57	23	60	-57	27
5 ($\geq 1000 \mu\text{g m}^{-3}$ removal)	76	-74	38	78	-75	44

The absolute bias increases with the magnitude of truncation or removal, from -14 % (situation 1) to -74 % (situation 5). Even without bias correction, the accuracy error is below 25 % for both the original data (situation 1) and the data truncated to $6553.4 \mu\text{g m}^{-3}$ (situation 2). Under situation 2, the absolute bias of the SPS30 is larger than the SEN55, which is further confirmation that the SEN55 measures higher concentrations than the SPS30. When removing all values $\geq 6553.4 \mu\text{g m}^{-3}$ (situation 3), bias correction is required to have accuracy errors below 25 %. Truncating to $1000 \mu\text{g m}^{-3}$ or removing these values altogether results in accuracy errors larger than the NIOSH threshold of 25 %. For indoor high-concentration circumstances, measurement values beyond the specified measurement range ($1000 \mu\text{g m}^{-3}$) are required for an accurate representation of the concentration. The fact that accuracy improves upon inclusion of these values, shows that both the SPS30 and the SEN55 can be used under higher concentrations than their specified measurement range.

3.5 Effect of relative humidity

Across eight relative humidity bins of 10 % (12.5 % to 92.5 %), the average SEN55 to SPS30 ratio varied between 1.10 and 1.14 (Fig. F1). There is no significant trend in the SEN55 to SPS30 ratio with an increase in relative humidity. This implies that the SEN55 and SPS30 are affected similarly by relative humidity.

In the SEN55 to gravimetry ratios there are no significant trends with increasing relative humidity (Appendix F.2). When correcting SEN55 data with Eq. (5) for GF(RH), there is a small but significant negative trend in SEN55 to gravimetry ratios (Appendix F.2). A physical correction for hygroscopic growth leads to an increasing underestimation with increasing relative humidities.



4. Discussion

395 4.1 Pragmatic air quality monitoring in Ethiopia

This study compared the performance of two Sensirion low-cost particulate matter sensors—SPS30 and SEN55—under ambient and indoor conditions in Arba Minch, Ethiopia. The results demonstrate that both sensors achieved high precision, accuracy, and stability across a wide range of concentrations, fulfilling the requirements for indicative and fixed reference-grade measurements (European Commission, 2010; NIOSH, 2012). Our findings advocate for a pragmatic shift in the
400 ‘monitoring hierarchy’, particularly for resource-constrained settings like Ethiopia. Traditionally, REMs are viewed as inherently superior, yet data does not always support this. For instance, the MCERTS certification of the Palas Fidas 200 showed the requirement of slope correction and expanded uncertainties up to 22.3 % (CSA Group Testing UK Ltd, 2024), while that of the uncorrected SPS30 data for its MCERTS certification ranged up to 8.9 %. Vogt et al. (2021) report for the Palas Fidas a slope and offset of 1.54 and -2.13 versus gravimetry, and a root mean squared error (RMSE) of 2.59 versus for
405 the SPS30 1.92 – 2.26. Tryner et al. (2020) use the TEOM as reference for the SPS30, but need to apply gravimetric corrections to the TEOM itself. Rabuan et al. (2023) validate the SPS30 with a TOPAS due to the latter being MCERTS certified, but that MCERTS certification is under lower concentrations ($< 18 \mu\text{g m}^{-3}$) and with a significantly higher resulting expanded uncertainty (32.2 %) than that of the SPS30 itself (CSA Group Testing UK Ltd, 2025b). These examples highlight that some ‘reference’ instruments introduce errors comparable to the sensors they are meant to validate, making it difficult to justify their
410 high capital and maintenance costs.

In comparison to high-cost REM installations, the high precision and linear response of the SPS30 and SEN55 allow for a more sustainable, locally-managed strategy: deploying such sensors ‘as-is’ and applying calibration factors retrospectively by moving mobile gravimetric units across different regions. Prioritizing long-term OEM sensor stability and simple linear corrections over proprietary ‘black-box’ systems and sparse REM installations ensures that limited budgets expand geographic
415 coverage and provide ‘higher truth’ rather than merely higher-cost data.

4.2 Concentration levels in ambient and indoor environments

The outdoor concentrations in our study (average: $15 \mu\text{g m}^{-3}$; range: $4\text{--}33 \mu\text{g m}^{-3}$) align with previous ambient SPS30 validation studies, which typically report means between 7 and $35 \mu\text{g m}^{-3}$ (Dingemanse and Tademe, 2023; Gäbel et al., 2022; Hassani et al., 2023; Hofman et al., 2022b; Hong et al., 2021; Park et al., 2021b). However, this study represents the first extensive
420 SPS30 and SEN55 validation in Ethiopia involving a mixture of traffic, biomass, and open waste burning. Compared to urban centers like Addis Ababa, with reported daily averages up to $66 \mu\text{g m}^{-3}$ and $80 \mu\text{g m}^{-3}$, our measured ambient ranges represent the lower end of the Ethiopian urban spectrum (AirNow Department of State, 2023; Tefera et al., 2021).

In contrast, indoor validation occurred under high concentrations: gravimetric samples reached $2000 \mu\text{g m}^{-3}$, with hourly peaks up to $10\,000 \mu\text{g m}^{-3}$. These levels significantly exceed the sensors’ specified range. Aside from earlier work in Arba Minch
425 (Dingemanse and Tademe, 2023), few studies have tested the SPS30 or SEN55 under such conditions. We found other indoor



validations up to 260 and 500 $\mu\text{g m}^{-3}$ (Penchala et al., 2025; Streuber et al., 2022), and only laboratory studies in a range similar to our study (Findlay et al. (2022): 1400 $\mu\text{g m}^{-3}$; Sousan et al. (2021): 1250 $\mu\text{g m}^{-3}$; Zaid et al. (2023): 3000 $\mu\text{g m}^{-3}$). Despite being ‘out of range’, these concentrations reflect the reality of Ethiopian households using biomass fuels, where peaks of 3000–4000 $\mu\text{g m}^{-3}$ are common (Admasie et al., 2019; Tamire et al., 2021).

430 4.3 Precision of SPS30 and SEN55 sensors

Both the SPS30 and SEN55 demonstrated high precision, with results meeting international benchmarks for reference-grade measurements. The between-sampler uncertainty (u_{bs}) for the SPS30 (0.23–1.4 $\mu\text{g m}^{-3}$) and SEN55 (1.3–1.5 $\mu\text{g m}^{-3}$) remained well below the European Commission’s 2.5 $\mu\text{g m}^{-3}$ threshold (2010). Similarly, the coefficient of variation (CV) for both sensors (1.4–5.1 %) was significantly lower than the 10 % limit recommended by the EPA and NIOSH. While some studies have reported higher CVs (e.g., Shittu et al. at 17.7 % (2025)), these are often attributed to single faulty units; our findings align more closely with studies finding u_{bs} values of 0.3 – 1.65 $\mu\text{g m}^{-3}$ and CV values < 10 % (CSA Group Testing UK Ltd, 2025a; Dingemane and Tademe, 2023; Hofman et al., 2024; Penchala et al., 2025).

Crucially, this high precision persisted at concentration readings well beyond the sensors’ specified range (> 1,000 $\mu\text{g m}^{-3}$). This reinforces findings from laboratory studies using woodsmoke (Tryner et al., 2020) and coal dust (Zaid et al., 2023), which noted strong R^2 values (0.94) at concentrations up to 20 000 $\mu\text{g m}^{-3}$. Nguyen et al. (2021) find for smoke under laboratory conditions higher CVs (16.6 %), while Sousan et al. 2021 find a low CV for salt (6.7 %), but 18.7–19.7 % for Arizona road dust (ARD) and oil mist. Our study is the first to confirm that this precision holds under real-world Ethiopian conditions for the SPS30 and provides the first documented precision data for the SEN55. Findings of high precision for the SPS30, as referenced by others (Gabriel and Auer, 2023; Mahajan, 2022; Mujan et al., 2021; Park et al., 2021a, b; Riediker, 2022), extends to the conditions of our study, as well as to the SEN55.

Our results demonstrate that precision can be further enhanced by accounting for individual sensor variations. Precision is often viewed as an inherent hardware trait, but factory calibration is a common part of measurement hardware. Factory calibration is fundamentally similar to an additional on-site calibration factor applied by an end-user integrating the OEM sensor into a larger system. Whether a calibration factor is determined by the manufacturer during a final check or by a user during on-site integration, the goal of correcting for sensor-specific variance remains the same.

4.4 Accuracy relative to gravimetric measurements

4.4.1 Outdoor accuracy

Under outdoor conditions, both sensors exhibited strong correlations with gravimetric measurements ($r = 0.89 - 0.91$, $R^2 = 0.99$). However, the raw data showed a systematic underestimation of $\text{PM}_{2.5}$ concentrations, with negative biases of approximately 17 – 20 % for the SPS30 and 11 % for the SEN55. This resulted in correction factors (slopes) of 1.20 – 1.24 and 1.12, respectively. Post-correction, accuracy errors (AE; 6.3 – 10.3 %) and expanded uncertainty (W_{CM} ; 8 – 12 %) fell



well within the 25 % criterion for fixed reference-grade measurements. In contrast to our findings, some European urban studies report slopes closer to 1.0 and W_{CM} values of 8.9% and 12.2% for uncorrected data (CSA Group Testing UK Ltd, 2025a; Hofman et al., 2022a; Shittu et al., 2025). This discrepancy could stem from factory calibrations performed at higher relative humidities; in our study area's drier climate, reduced hygroscopic growth likely drives the negative bias. Nevertheless, similar underestimations have been documented elsewhere, including outdoor slopes of 1.09-1.23 in Norway (Vogt et al., 2021), a factor of 1.15 in the Netherlands (Wesseling et al., 2021) and laboratory-confirmed out-of-box bias (Hofman et al., 2024).

4.4.2 Indoor accuracy

Both sensors maintained high linearity under indoor conditions ($R^2 = 0.96 - 0.99$), even with concentrations going well beyond the sensor specification range. Average slopes of 1.14 (SPS30) and 1.15 (SEN55) align with a reanalysis of previous findings in Arba Minch (1.13; Appendix G). Notably, the lack of non-linear behavior at these high concentrations argues against instrumental saturation. Following correction, AE values remained below the 25 % threshold. The slightly higher errors found indoors relative to outdoors may be partially attributed to the reference sampler's own uncertainty (UPAS expanded uncertainty estimated at 12.2 %). While Zaid et al. (2023) reported poor SPS30 response to coal dust above $1000 \mu\text{g m}^{-3}$, our results match the robust linearity found by Sousan et al. (2023) for concentrations up to $15\,000 \mu\text{g m}^{-3}$. The observed indoor slope variations (1.01 – 1.25) are likely attributable to local spatial heterogeneity; Gaussian plume modelling suggests that a 0.3 m shift from the plume center is 16 % (and from 0.3 to 0.6 m relative to plume center 41 %), a margin consistent with the individual slope variations.

4.4.3 Accuracy and particle composition

Compositional differences likely drive the lower slopes (lesser underestimation) observed indoors (1.14) compared to outdoors (1.21). This shift mirrors laboratory findings where the SPS30 reports higher values for wood smoke than for salts or mineral dust (Tryner et al., 2020). However, whereas Tryner et al. reported wood smoke overestimation (slope 0.6) and high variation across aerosols (0.6 – 2.1), our sensors continued to underestimate concentrations and remained relatively stable across environments (1.14 vs 1.21).

The relative stability suggests that real-world Ethiopian biomass emissions differ significantly from laboratory-grade smoke and that the sensors are more consistent under field conditions than controlled experiments might imply. To further isolate the sensor response to real-world biomass fuel particles, future research could either conduct continuous validation against high-resolution reference monitors to assess peak-level performance beyond filter-averaged data, or evaluate performance at lower ambient concentrations in residential areas with high biomass usage to evaluate the influence of aged or diluted smoke.



4.5 Equivalence between SPS30 and SEN55

Direct comparison of collocated SPS30 and SEN55 units revealed high inter-model agreement. Without correction, between-sensor uncertainties (u_{bs}) were 1.0–3.0 $\mu\text{g m}^{-3}$, within the range for indicative sampling ($\leq 5 \mu\text{g m}^{-3}$). Under outdoor conditions, a significant difference in slopes was observed (SPS30 = 1.21; SEN55 = 1.11). After adjusting for this slope difference, u_{bs} decreased to 0.41–0.72 $\mu\text{g m}^{-3}$ and the CV dropped from ~8% to 3–4%. This demonstrates that the two sensors are functionally equivalent once calibration offsets are accounted for.

The ‘SEN55-higher’ trend persisted across indoor conditions (SPS30/SEN55 ratios of 0.92–0.93) and was corroborated by a 0.94 slope found during four months of background measurements in Sweden (Appendix H). While Rodríguez Rama et al. (2024) and Rabuan et al. (2023) similarly noted higher readings from the SEN54/55 compared to the SPS30, our study is the first to quantify these slopes across diverse environments. The SEN55’s reduced outdoor underestimation (11 % versus 17 – 20 % for SPS30) suggests a potential factory refinement to the OEM calibration. Provided the systematic ratio between them is recognized, both sensor types are suitable for mixed deployment in monitoring networks, and existing SPS30 performance literature can be extended to the SEN55.

4.6 High-concentration events and sensor stability

Both sensors remained stable and precise following repeated exposures to high concentrations ($> 1000 \mu\text{g m}^{-3}$), corroborating laboratory findings by Tryner et al. (2020) where SPS30 precision held after exposures up to 33 000 $\mu\text{g m}^{-3}$. However, a key functional difference emerged: SEN55 measurements are digitally truncated at 6553.4 $\mu\text{g m}^{-3}$, whereas the SPS30 continues to record higher values. Statistical testing (Pearson χ^2 , $p \ll 0.001$) confirmed that these SEN55 truncation events corresponded accurately with the SPS30’s peak readings, suggesting these peaks are true physical occurrences rather than sensor noise.

Importantly, our results demonstrate that including values beyond the 1000 $\mu\text{g m}^{-3}$ manufacturer specification is essential for maintaining accuracy in high-emission environments; truncating or removing data at that limit would result in unacceptably large accuracy errors. The SEN55 digital truncation did not lead to unacceptable accuracy errors, indicating that SEN55 data remain valid for the measurement range of our study. Because our validation included filter averages up to 2000 $\mu\text{g m}^{-3}$ (encompassing even higher instantaneous peaks), the sensors have been tested under conditions that exceed the average concentrations typically reported for biomass-burning environments in Ethiopia (405 $\mu\text{g m}^{-3}$; Enyew et al. (2023)), China (85 – 658 $\mu\text{g m}^{-3}$; Hu et al. (2014)), and across Africa (up to 550 $\mu\text{g m}^{-3}$; Safo-Adu et al. (2023)). This confirms that both sensors are validated for the full range of concentration levels likely to be encountered in real-world biomass fuel indoor air pollution studies.

The robust linear relationship found between filter and sensor averages further suggests that potential high-concentration errors are minimal. Theoretically, issues such as coincidence (leading to undercounting) or aerosol residuals (leading to overestimation) would manifest as non-linear behavior, with errors compounding at higher concentrations. While we cannot verify the accuracy of raw 1-second peaks, the consistent reporting of high values at 10-minute averaged levels across both



sensor types indicates these measurements are meaningful. Pragmatically, exposure studies generally prioritize 24-hour averages over short-term plumes; our results confirm that for these relevant timescales, the sensors provide a valid and reliable representation.

4.7 Effect of relative humidity

We found no evidence of a relative humidity (RH) effect on the SPS30-to-SEN55 ratio in either Ethiopia or during four months of background monitoring in Sweden (Appendix H). This indicates that both sensors respond to RH similarly. While we found a slight trend between SEN55 and gravimetric measurements relative to RH, applying a correction based on κ -Köhler theory ($\kappa = 0.3$) resulted in a reversed trend. This implies a slight underestimation by the correction, possibly because the assumed κ -factor is too high for aerosols in our study area. Particles from open waste and biomass burning typically exhibit lower hygroscopicity, with studies reporting values between 0.01–0.19 (Kreidenweis and Asa-Awuku, 2014) and specifically 0.06–0.07 for Sub-Saharan the typical Sub-Saharan biomass fuels eucalyptus and cow dung (Mouton et al., 2023). Rissler et al. (2010) suggest a slightly lower value (0.26) for biomass burning regions.

No underestimation was observed when applying κ -Köhler correction to background measurements in Sweden (Appendix H). We conducted the corrections with the SEN55 measured RH, which were lower than collocated reference instrumentation, both in our study area and in Sweden (Appendix H). A likely partial explanation of lower SEN55 RH measurements is sensor self-heating. Using the reference measurements in the κ -Köhler correction lead to a significant overcorrection (Appendix H), which suggests that internal RH is more representative of the conditions particles experience.

Our results align with literature showing that the SPS30 appears less reactive to ambient RH fluctuations compared to other OEM sensors. For instance, Tryner et al. (2020) found that standard RH corrections led to an underestimation at high RH, while Hassani et al. (2023) observed only a slight mean bias increase ($\sim 1 \mu\text{g}/\text{m}^3$) across the 60–100 % RH range. Hong et al. (2021) noted that while Plantower and Honeywell sensors showed high fluctuations at increasing RH, the SPS30 bias increased only slightly above 80 %, and Vogt et al. (2021) found that sensor systems with an SPS30 showed lowest dependence on RH changes. These findings are likely due to the use of ambient RH in those studies, where the internal sensor RH – lowered by self-heating – explains the diminished hygroscopic response.

In Arba Minch, daily average RH is generally below 80 % and was consistently under 70 % during our gravimetric sampling. Given the sensor's low sensitivity in this range and the likely low hygroscopicity of local biomass particles, we do not expect RH to cause significant accuracy errors in cities with similar climatology. While further research is required to validate performance in Ethiopian regions with higher average relative humidities, the commonality of biomass sources suggests that low particle hygroscopicity may be a shared characteristic. This is a favorable outcome for Ethiopian monitoring: since reference-grade RH data is scarce, the limited need for complex RH-dependent corrections reduces the resource burden for maintaining accurate data.



5. Conclusions

550 This study provides the first validation of Sensirion SPS30 and SEN55 sensors against gravimetry under outdoor and indoor conditions in an Ethiopian city. Despite concentrations frequently exceeding manufacturer specifications, both sensors demonstrated high stability and precision ($u_{bs} < 1.72 \mu\text{g m}^{-3}$, $CV < 7.7 \%$). After applying site-specific correction factors, the sensors met sampling guidelines for accuracy, with outdoor errors below 11 % and indoor errors below 22 %.

A significant finding is the functional equivalence of the SPS30 and SEN55 once inter-model offsets are addressed. While the
555 SEN55 consistently reports higher values than the SPS30, adjusting for this trend yields nearly identical precision metrics ($u_{bs} < 1.3 \mu\text{g m}^{-3}$; $CV < 3.1 \%$). This equivalence holds until the SEN55 reaches its digital truncation limit of $6553.4 \mu\text{g m}^{-3}$. Critically, we find that measurements exceeding $1000 \mu\text{g m}^{-3}$ are not random noise but meaningful data; ignoring or truncating values at the $1000 \mu\text{g m}^{-3}$ threshold leads to unacceptably large accuracy errors and an inability to represent the true exposure concentrations under biomass-burning conditions.

560 Furthermore, while relative humidity (RH) does influence readings, the effect is less pronounced than predicted by standard κ -Köhler, likely due to a combination of lower hygroscopicity of local biomass aerosols and lesser effect of the Sensirion sensors. This suggests that in climates similar to Arba Minch, the SPS30 and SEN55 sensors can provide reliable data without the need for complex, resource-heavy RH corrections.

To further refine the use of low-cost sensors in Ethiopia, future research should prioritize:

- 565
- Hygroscopicity studies: investigating the specific hygroscopicity of Ethiopian biomass aerosols to better understand RH effects on particle measurements.
 - Expanded environmental validation: conducting measurements under higher outdoor background concentrations (e.g., Addis Ababa) and higher RH regimes to establish broader regional correction factors.
 - High-resolution monitoring: utilizing higher time-frequency validation under biomass burning conditions to gain
570 deeper insight into the differing correction factors for indoor versus outdoor concentrations.

However, the most critical recommendation is to move from validation to active monitoring. Our results indicate that the SPS30 and SEN55 are already sufficiently precise and stable for large-scale application. In resource-constrained settings, limited budgets are most effectively spent by:

- 575
- Starting deployment now: utilizing these sensors immediately to build the high-density networks required to mitigate air pollution, rather than waiting for further refinement.
 - Prioritizing mobile gravimetry: investing in mobile gravimetric units for validation across the country, which offers higher accuracy and better value than a few stationary reference-equivalent monitors.
 - Local capacity building: instead of importing proprietary 'black-box' systems, integrating OEM sensors into locally-built systems to save costs, preserve raw data (avoiding 'averaging-away' high peaks), and foster technical self-
580 reliance.

<https://doi.org/10.5194/egusphere-2026-2537>

Preprint. Discussion started: 11 June 2026

© Author(s) 2026. CC BY 4.0 License.



Ultimately, the SPS30 and SEN55 provide a robust, cost-effective path toward understanding the air quality challenges in Ethiopia, provided they are supported by pragmatic validation strategies.



Appendix A Measurement installations

A.1 Sensor systems

585 Figure A1 shows the SPS30 and SEN55 sensors.

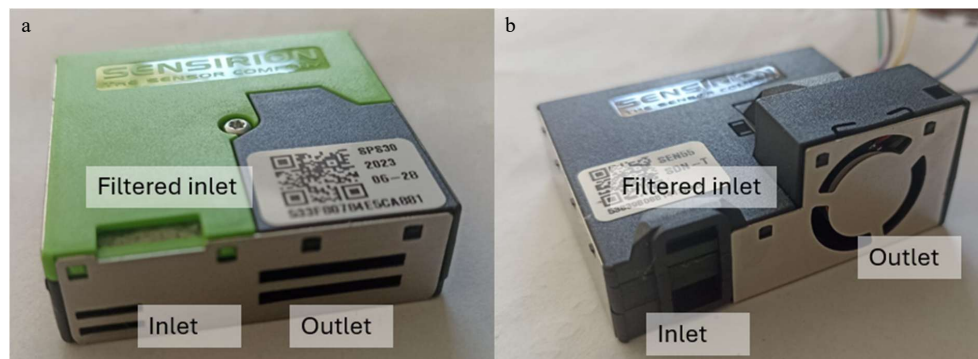
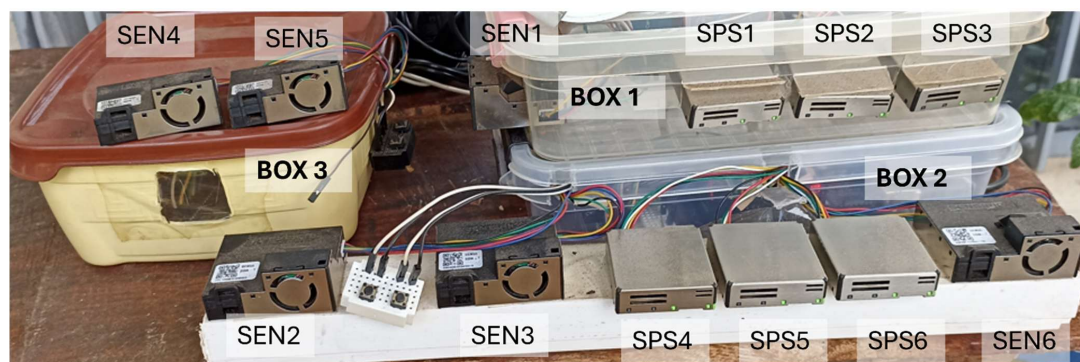


Figure A1: SPS30 (a) and SEN55 (b) sensors.

The sensors were all connected to microprocessors (Arduino Mega or ESP32). The following set-ups were used:

- Box 1: three SPS30 and one SEN55, connected to an Arduino Mega, sensors sticking out of the box (SPS1-3, SEN1).
- 590 - Box 2: three SPS30 and one SEN55 on one Arduino Mega (SPS4-6, SEN6), and two SEN55 connected to two ESP32 (SEN2, SEN3). The six sensors were placed on a railing in front of the box.
- Box 3: two SEN55 to ESP32 individually (SEN4, SEN5) sensors placed on the top of the box.

Figure A2 shows all sensor systems used in this study.



595 Figure A2: Overview of three boxes with all SPS30 and SEN55 sensors used across this study.

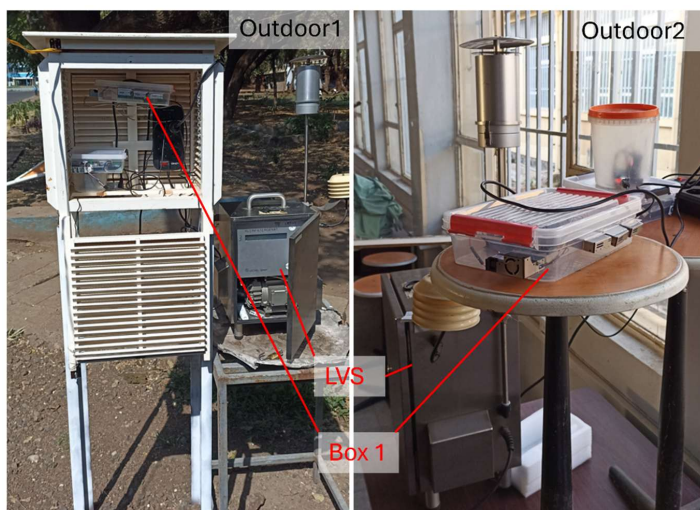
All microprocessors had an SD module for data storage and DS3231 Real Time Clock. The Arduino Mega clock modules were set manually, while the ESP32 modules retrieved their time from an internet time server.



A.2 Field installations

Location Outdoor 2 is technically installed indoor, inside a lab behind an open window. There are no sources inside the lab, except for the occasional resuspension of particulate matter when persons are visiting the lab. At location Outdoor 2, there were a distinct morning and evening peak in the same order of magnitude as at location Outdoor 1 (Fig. D1). We therefore assume that concentrations at Outdoor 2 are from similar sources as at Outdoor 1, and for this reason use data of both locations as one ‘outdoor’ dataset.

At location Outdoor 1, the LVS was placed at a height of one meter, and box 1 was placed in a wooden box for weather protection. At Outdoor 2, the LVS and box 1 were placed at similar heights close to windows of the lab. At Kitchen 1 and 2, the sensor boxes and UPAS instruments were placed in a metal cage at a height of 2 meters. At location Residence, the sensor boxes were placed at the front entrance behind metal mesh with direct communication with the outdoor air, at a height of 2.20 meters. Figures A3 through A6 show the installations at all locations.



610 **Figure A3: Sensor and gravimetric instrument installations at locations Outdoor 1 and 2.**



Figure A4: Sensor and gravimetric instrument installations at location Kitchen 1.

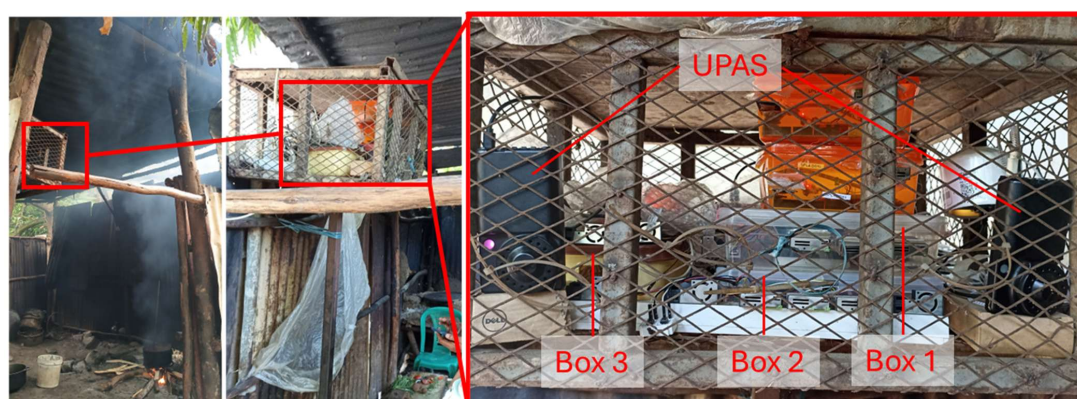


Figure A5: Sensor and gravimetric instrument installations at location Kitchen 2.



615

Figure A6: Sensor installations at location Residence.

A.3 Data management

SPS1 encountered a period of malfunctioning, after which data has been left out. Due to an unreliable battery pack, the microprocessor of SPS1-3 and SEN1 caused spurious results. This data has been left out.



620 In comparison with gravimetric measurements, phase 2 data of SEN1 and SEN2 are ignored. SEN1 was positioned perpendicular to all other sensors and gravimetric measurements (Fig. A2). Under high concentrations, sensor orientation affects the measurements (Zaid et al., 2023). Due to power problems SEN2 encountered data loss and was left with only 6 valid pairings. Therefore, in comparison with gravimetric measurements, phase 2 data of SEN1 and SEN2 are ignored.



625 **Appendix B Gravimetry**

B.1 Standard deviation of analytical balance

As per the user manual, the readability (standard deviation) of the AE240 analytical balance is 20 µg (IET, n.d.). The analytical balance at the Arba Minch University lab is not included in an official calibration scheme. Instead, with every weighing moment, control weights weighed along. Since February 2025, three pieces of aluminium foil are used as control weights.

630 Figure B1 shows all weights across 75 weighing moments.

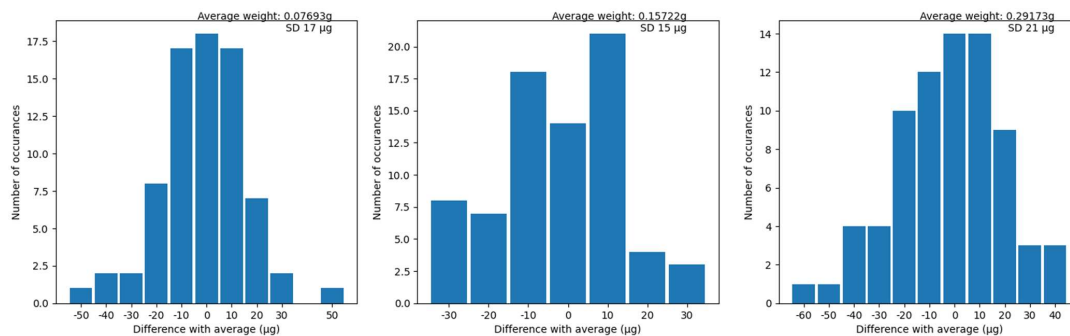


Figure B1: Weight results (n=75) of three control weights, relative to their average weight.

Across 75 weighing moments, the standard deviations for the three control weights are 17, 15 and 21 µg, respectively. We can therefore assume that the standard deviation as provided by the instrument manufacturer is correct, and that the analytical balance operates as expected.

635

B.2 Gravimetric procedures

Standard protocol involved three or more pre- and post-sampling weighings, though 27 filters subject to load-capacity testing received single intermediate weighings. Both dedicated blanks and unused sampling filters were used for correction. During a rainy period at the Outdoor 1 site (27 March –11 April), three sampling filters were repurposed as field blanks to control for humidity-induced weight discrepancies between the field and the laboratory.

640

To determine the final mass, the differences between all possible pre- and post-sampling weight combinations were calculated and averaged. These values were then corrected using the mean mass change observed in the corresponding blanks.

Based on the standard deviation of the analytical balance (20 µg, see section B.1) and the above calculation, we calculated a theoretical standard deviation SD_T of the $PM_{2.5}$ weight with Eq. (B1):

645
$$SD_T = \sqrt{SD_{field}^2 + SD_{blank}^2} \tag{B1}$$

where SD_{field} and SD_{blank} are calculated with Eq. (B2) and Eq. (B3):



$$SD_{field} = \sqrt{\frac{20^2}{N_{Pre}} + \frac{20^2}{N_{Post}}} \tag{B2}$$

$$SD_{blanks} = \frac{\sqrt{\frac{20^2}{N_{pre}} + \frac{20^2}{N_{post}}}}{\sqrt{N_{Blanks}}} \tag{B3}$$

With N_{pre} and N_{post} being the number of pre- and post-weighings, and N_{Blanks} the number of blanks. Table B1 shows an overview of all gravimetry numbers and results.

Table B1: Overview of all gravimetric measurements, with number of pre-weighings (Pre), post-weighings (Post), blanks (B), location, sample period (Start, End), hours of power interruption (PI) during the sample, sampled volume, blank-corrected weight and theoretical standard deviation of the weight (SD_T) across pre- and post-weighing pairings. SD_T is given in µg, and in percentage relative of the total weight.

Filter code	Pre	Post	B	Location	Start	End	PI ⁺ hour	Volume m ³	Weight µg	SD _T µg	SD _T %
L01	1	8	3	Lab	2024-12-31 17:29	2025-01-01 21:05	3.62	55.18	944	24	2.5
L02	1	7	3	Lab	2025-01-02 15:19	2025-01-03 15:19		55.19	854	25	2.9
L03	2	6	3	Lab	2025-01-04 17:17	2025-01-05 17:17		55.19	824	19	2.3
L04	1	6	3	Lab	2025-01-06 17:50	2025-01-07 17:50		55.19	1262	25	2.0
L05	2	5	3	Lab	2025-01-08 15:02	2025-01-09 15:12	0.18	55.19	1112	19	1.7
L06	2	5	4	Gate	2025-01-10 15:21	2025-01-11 12:00		47.56	904	19	2.1
L07	2	5	4	Gate	2025-01-11 12:13	2025-01-12 12:21	0.13	55.22	1024	19	1.9
L08	2	5	4	Gate	2025-01-12 14:01	2025-01-13 14:01		55.19	1100	19	1.7
L09	2	5	4	Gate	2025-01-13 17:44	2025-01-14 17:29	0.35	53.84	1623	19	1.2
L10	2	5	4	Gate	2025-01-14 17:52	2025-01-15 17:52		55.19	1676	19	1.1
L11	2	5	4	Gate	2025-01-15 18:19	2025-01-16 18:11		54.79	1381	19	1.4
L12	2	5	4	Gate	2025-01-16 18:18	2025-01-17 16:13		50.40	1136	19	1.7
L13	3	1	3	Lab	2025-01-29 14:35	2025-01-30 10:44		46.35	970	27	2.8
L14	1	11	3	Lab	2025-01-30 10:59	2025-01-31 9:51	0.18	52.16	932	24	2.6
L15	4	8	4	Lab	2025-01-31 10:14	2025-02-01 10:51	0.4	55.68	1012	14	1.4
L16	8	5	3	Lab	2025-02-03 9:04	2025-02-04 9:29	0.22	55.64	1293	13	1.0
L17	10	3	3	Lab	2025-02-04 16:56	2025-02-05 16:26	0.32	53.34	1225	15	1.2
L18	1	1	8	Lab	2025-02-06 9:20	2025-02-07 9:03	0.17	54.14	1193	30	2.5
L19	1	1	8	Lab	2025-02-07 9:27	2025-02-08 9:41	0.23	55.19	880	30	3.4
L20	1	1	8	Lab	2025-02-10 9:36	2025-02-11 8:40	0.33	52.29	714	30	4.2
L22	1	1	8	Lab	2025-02-12 16:58	2025-02-13 16:48		54.80	494	30	6.1
L23	1	13	6	Lab	2025-02-13 17:17	2025-02-14 15:32	0.03	51.03	828	22	2.7
L24	8	1	7	Lab	2025-02-17 10:05	2025-02-18 9:12		53.14	1217	23	1.9
L25	1	1	7	Lab	2025-02-18 9:17	2025-02-19 10:11	0.35	56.45	1214	30	2.5
L26	1	1	7	Lab	2025-02-19 10:15	2025-02-20 8:48		51.81	1204	30	2.5
L27	1	8	5	Lab	2025-02-20 8:51	2025-02-21 8:49	0.08	54.90	1056	23	2.2
L28	12	7	5	Lab	2025-02-21 9:39	2025-02-24 8:53	0.18	163.31	2943	10	0.3
L29	13	1	5	Lab	2025-02-24 10:19	2025-02-25 8:58	0.03	52.01	784	23	2.9
L30	1	1	5	Lab	2025-02-25 9:02	2025-02-26 8:25	0.08	53.54	1032	31	3.0
L31	1	1	5	Lab	2025-02-26 8:29	2025-02-27 12:07		63.52	1316	31	2.4
L32	1	8	4	Lab	2025-02-27 12:10	2025-02-28 14:01	0.43	58.35	1614	24	1.5
L33	17	1	4	Lab	2025-02-28 14:57	2025-03-01 10:57	1.27	43.02	1115	23	2.1
L34	1	6	5	Lab	2025-03-01 11:00	2025-03-03 8:27	2	99.84	2120	24	1.1
L35	4	1	4	Lab	2025-03-03 11:24	2025-03-04 9:32		50.91	1321	25	1.9
L36	1	1	4	Lab	2025-03-04 9:36	2025-03-05 9:48	0.32	54.91	1053	32	3.0
L37	1	9	4	Lab	2025-03-05 9:51	2025-03-06 16:09		69.61	1356	24	1.8
L38	6	1	5	Lab	2025-03-06 16:14	2025-03-07 16:53	0.12	56.41	1306	24	1.8
L39	1	7	5	Lab	2025-03-07 16:56	2025-03-10 7:53	2	140.07	2354	23	1.0
L40	6	1	4	Lab	2025-03-10 9:22	2025-03-11 16:14	8.85	50.42	661	24	3.6
L41	1	1	4	Lab	2025-03-11 16:18	2025-03-12 13:54		49.67	740	32	4.3
L42	1	4	4	Lab	2025-03-12 13:58	2025-03-14 5:36	14.82	56.73	872	25	2.9
L43	8	1	4	Lab	2025-03-14 10:10	2025-03-15 10:31		55.99	1064	24	2.3



L44	1	3	4	Lab	2025-03-15 10:34	2025-03-17 8:18	1.08	102.65	1803	26	1.4
L45	4	7	1	Gate	2025-03-27 16:42	2025-03-28 16:24	1.52	51.02	629	18	2.9
L46	4	7	1	Gate	2025-03-28 16:48	2025-03-29 16:48		55.21	789	18	2.3
L47	4	7	1	Gate	2025-03-31 8:38	2025-04-01 8:38		55.10	1002	18	1.8
L48	4	7	1	Gate	2025-04-01 12:16	2025-04-02 14:25	2.15	55.17	957	18	1.9
L49	4	7	4	Gate	2025-04-03 17:13	2025-04-04 17:03		54.82	2737	14	0.5
L50	4	4	2	Gate	2025-04-04 17:14	2025-04-06 1:30	8.8	55.20	776	17	2.2
L51	4	4	2	Gate	2025-04-07 17:38	2025-04-08 17:38		55.18	1009	17	1.7
L52	4	4	2	Gate	2025-04-08 17:51	2025-04-09 17:10	0.08	53.46	1096	17	1.6
L53	4	4	2	Gate	2025-04-09 17:20	2025-04-10 17:12	0.25	54.29	1011	17	1.7
L54	4	4	2	Gate	2025-04-10 17:22	2025-04-11 17:22		55.20	894	17	1.9
L55	4	4	2	Gate	2025-04-11 17:51	2025-04-13 1:48	7.97	55.17	791	17	2.1
U01	4	4	4	Kitchen1	2025-06-09 15:33	2025-06-10 15:15		1.42	344	16	4.7
U02	4	4	4	Kitchen1	2025-06-10 15:45	2025-06-11 15:11		1.41	141	16	11.3
U03	4	4	4	Kitchen1	2025-06-11 15:36	2025-06-12 15:22		1.43	181	16	8.8
U04	4	4	4	Kitchen1	2025-06-12 15:27	2025-06-13 15:03		1.41	309	16	5.2
U05	4	4	4	Kitchen1	2025-06-13 15:23	2025-06-14 15:17		1.43	261	16	6.1
U06	4	4	4	Kitchen1	2025-06-14 15:46	2025-06-15 15:10		1.40	131	16	12.2
U07	3	3	3	Kitchen1	2025-06-16 15:29	2025-06-17 15:10		1.42	129	19	14.7
U08	3	3	3	Kitchen1	2025-06-17 15:34	2025-06-18 15:13		1.42	99	19	19.2
U09	3	3	3	Kitchen1	2025-06-18 15:24	2025-06-19 15:08		1.42	92	19	20.7
U10	3	3	3	Kitchen1	2025-06-19 15:19	2025-06-20 15:07		1.43	49	19	38.8
U11	3	3	3	Kitchen1	2025-06-20 15:27	2025-06-21 19:31		1.68	69	19	27.5
U12	3	3	3	Kitchen1	2025-06-21 19:36	2025-06-22 17:55		1.34	29	19	65.5
U13	4	4	4	Kitchen2	2025-06-09 15:56	2025-06-10 15:58		1.44	2109	16	0.8
U14	4	4	4	Kitchen2	2025-06-10 16:16	2025-06-11 15:41		1.40	2571	16	0.6
U15	4	4	4	Kitchen2	2025-06-11 15:55	2025-06-12 15:33		1.42	2504	16	0.6
U16	4	4	4	Kitchen2	2025-06-12 15:46	2025-06-13 13:14		1.29	1894	16	0.8
U17	4	4	4	Kitchen2	2025-06-13 15:53	2025-06-14 15:51		1.44	2399	16	0.7
U18	3	3	3	Kitchen2	2025-06-16 15:44	2025-06-17 15:38		1.43	1742	19	1.1
U19	3	3	3	Kitchen2	2025-06-17 15:48	2025-06-18 15:31		1.42	2286	19	0.8
U20	3	3	3	Kitchen2	2025-06-18 15:47	2025-06-19 15:23		1.41	1486	19	1.3
U21	3	3	3	Kitchen2	2025-06-19 17:09	2025-06-20 15:33		1.34	1806	19	1.1
U22	3	3	3	Kitchen2	2025-06-20 16:02	2025-06-21 16:02		1.44	1446	19	1.3
U23	3	3	3	Kitchen2	2025-06-21 19:50	2025-06-22 18:04		1.33	589	19	3.2
U24	3	3	7	Kitchen2	2025-06-24 15:26	2025-06-25 3:26		0.72	921	17	1.8
U25	3	3	7	Kitchen2	2025-06-25 3:25	2025-06-25 15:03		0.70	588	17	2.9
U26	3	3	7	Kitchen2	2025-06-25 15:20	2025-06-26 3:20		0.72	784	17	2.2
U27	3	3	7	Kitchen2	2025-06-26 3:48	2025-06-26 14:59		0.67	1084	17	1.6
U28	3	3	7	Kitchen2	2025-06-26 15:23	2025-06-27 3:23		0.72	701	17	2.4
U29	3	3	7	Kitchen2	2025-06-27 3:28	2025-06-27 15:06		0.70	651	17	2.6
U30	3	3	7	Kitchen2	2025-06-27 15:29	2025-06-28 3:29		0.72	254	17	6.7
U31	3	3	7	Kitchen2	2025-06-28 3:33	2025-06-28 14:31		0.66	294	17	5.8

655 a: The LVS depends on a power supply, and stops operating during a power interruption. A power logger kept track of moments of power interruption. For filter to sensor comparison, this information was used to select only data from the sensors during which the LVS had been running.

B.3 Gravimetry data management

Eight filter measurements were excluded: L21 was removed due to LVS flow instability, L49 was identified as an outlier via Grubb's test at 99% confidence level, following GDE guidelines (European Commission, 2010), and filters U07-U12 were excluded because their theoretical standard deviation (Eq. (B1)) exceeded 12.5 % of total mass.

For sensor-to-filter comparisons, all data points between start- and end-times of filter sampling were used, excluding any periods of LVS power interruption. Sensor averages were only included if they maintained at least 90 % coverage of the 10-minute averages during the respective filter sampling period.



B.4 Gravimetric instruments uncertainty

- 665 According to the Guide for Demonstration of Equivalence (GDE), the maximum allowable uncertainty between two reference instruments such as the LVS is $2 \mu\text{g m}^{-3}$ (European Commission, 2010). This translates to $1.41 \mu\text{g m}^{-3}$ for one instrument, at one standard deviation (68 % confidence interval). The GDE expresses expanded uncertainty (uncertainty with a 95 % confidence interval) as percentage relative to a level of $30 \mu\text{g m}^{-3}$. $1.41 \mu\text{g m}^{-3}$ translates to 4.7 % uncertainty. The expanded uncertainty (95 % confidence interval) is then 9.4 %. The error of the LVS measurement is most likely lower. We expect the
- 670 main error components of the gravimetric measurements to be the gravimetry (filter weighing), and the instrument flow rate. For gravimetry with the LVS, the average standard deviation as percentage of filter weight (Table B1) was 2.2 %. Since the LVS is according to CEN EN 12341, the flow uncertainty is lower than 2 % (TUV SUD, 2025). These two main error components give a combined uncertainty of $\sqrt{2.2^2 + 2^2} = 3.0 \%$, implying an expanded uncertainty of 6.0 %. The absolute uncertainty at a level of $30 \mu\text{g m}^{-3}$ with 3 % is $0.9 \mu\text{g m}^{-3}$.
- 675 For gravimetry with the UPAS, the average standard deviation as percentage of filter weight (Table B1) was 8.8 %. We however excluded filters from the analysis with a standard deviation beyond 12.5 % (see section B.3). Without these filters, the average standard deviation becomes 3.5 %. As per company specification the flow uncertainty is 4 % (Access Sensor Technologies, 2024). This gives a combined uncertainty of $\sqrt{3.5^2 + 4^2} = 6.1 \%$, implying an expanded uncertainty of 12.2 %.

680

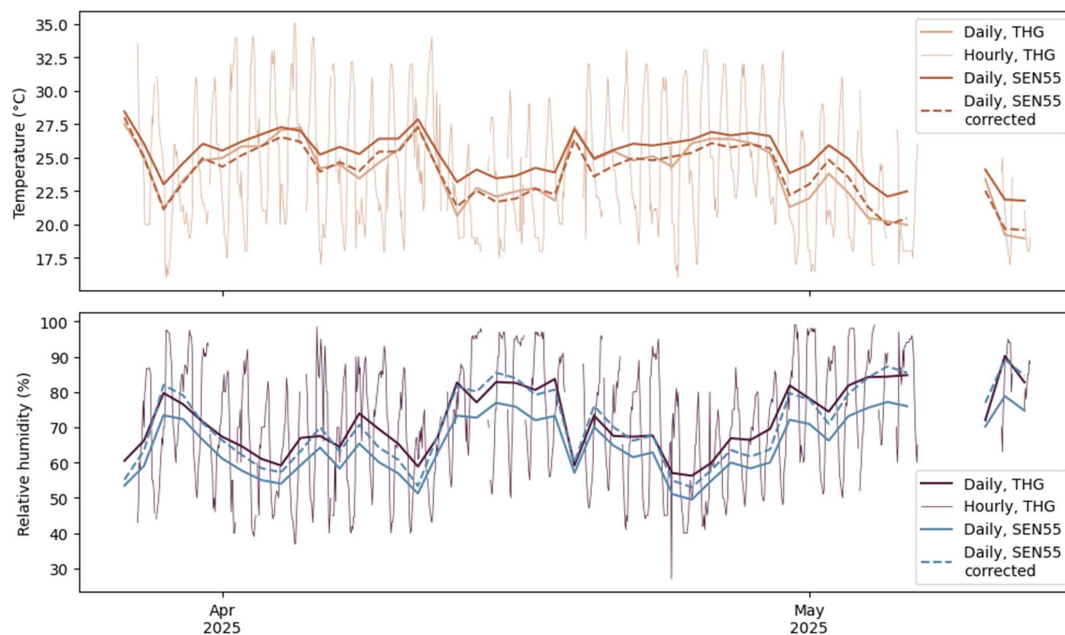


Appendix C Meteorology

C.1 SEN55 RH and T validation

C.1.1 Comparison with thermohygrograph

685 To validate SEN55 measurements of relative humidity (RH) and temperature (T), we collocated a thermohygrograph (THG) with the SEN55 at location Outdoor 1. A THG has an expected accuracy of 3 % and 1 K for RH and T, respectively (World Meteorological Organization, 2008). Figure C1 shows the temperature and relative humidity as measured by the THG and SEN55.



690 **Figure C1: temperature and relative humidity as measured by the thermohygrograph (THG) and SEN55. For the SEN55, corrected values (see section C.1.2) are also shown.**

At the same location, the daily averages of the SEN55 closely matched those measured by the THG (RMSE of daily averages for T and RH 1.5 °C and 7.1 %, r of 0.96 and 0.97, respectively).



C.1.2 Offset and slope of SEN55

695 The SEN55 relative to the THG measures higher temperatures and lower relative humidities (Fig. C1). We expect that the RH error is a direct (physical) result from the T error. This implies that based on a statistical temperature correction, RH can be corrected based on physical relations.

The Clausius-Clapeyron derivative substituted into an RH change to temperature change relation gives Eq. (C1):

$$\frac{\delta RH}{RH} \approx -\frac{L_v}{R_v T^2} \delta T \quad (C1)$$

700 In which L_v is the latent heat of vaporization (approximately $2.5 \cdot 10^6$ J kg⁻¹ in our temperature range with a molar mass of 18.015 g mol⁻¹) and R_v is the specific gas constant (461 J kg⁻¹ K⁻¹). In our temperature range of 288–308 K, $\frac{L_v}{R_v T^2}$ varies from 0.057 to 0.065. We therefore rewrite to Eq. (C2):

$$\Delta RH \approx -0.06 \cdot RH \cdot \Delta T \quad (C2)$$

With ΔT being $T_{SEN55} - T_{real}$.

705 We can rewrite to calculate $RH_{corrected}$ based on T_{SEN55} , RH_{SEN55} and an estimated T_{real} with Eq. (C3):

$$RH_{corrected} \approx RH_{SEN55} + 0.06 \cdot RH_{SEN55} \cdot (T_{SEN55} - T_{real}) \quad (C3)$$

We estimate T_{real} based on ordinary least squares (OLS) regression between T_{SEN55} and T_{THG} . This resulted in a slope of 1.27 and intercept of -8.0 ($R^2 = 0.85$). In other words, we calculated T_{real} with Eq. (C4):

$$T_{real} = 1.27 \cdot T_{SEN55} - 8.0 \quad (C4)$$

710 Figure C1 shows the corrected SEN55 data. With the corrected RH, the RMSE to RH_{THG} becomes 2.9 %. For the corrected T this is 0.62 °C. This is well within the compounded accuracy of the SEN55 specified and THG expected accuracies. Given that the physical RH correction resolves the RH error, RH seems accurately measured and the deviation from ambient is due to instrument heating.

C.1.3 Reasons for temperature offset

715 The significant slope and intercept of 1.27 and -8.0 (Eq. C4) indicate that the SEN55 overestimates temperatures, which becomes more pronounced at lower ambient temperatures (as illustrated in Fig. C1). Figure C2 shows the hourly temperature differences (SEN55-THG).

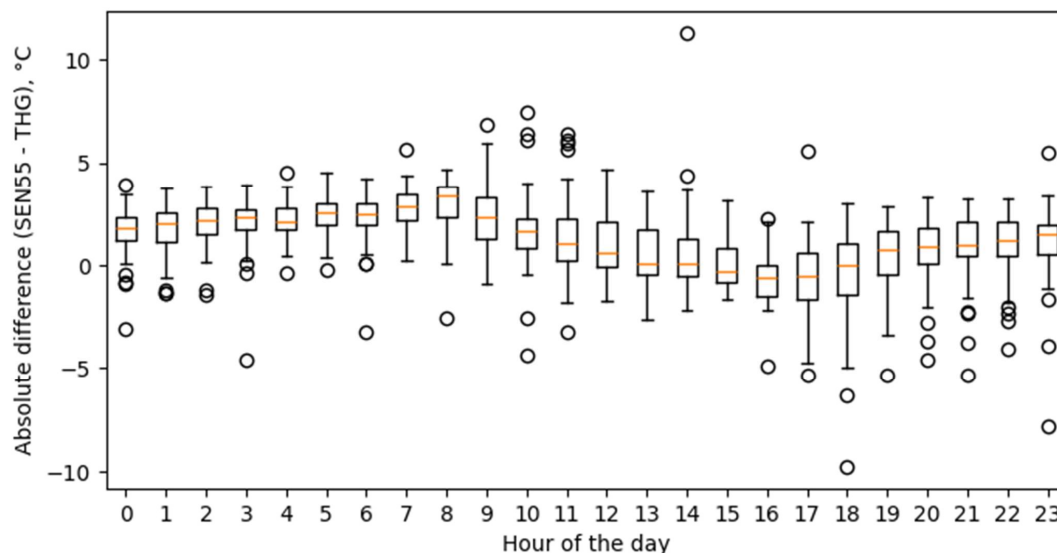


Figure C2: boxplots of hourly temperature differences between the SEN55 and THG measurements (SEN55 – THG).

720 The hourly temperature difference shows a diurnal pattern (Fig. C2): the average error peaks during nighttime, coinciding with lower ambient temperatures and reduced ventilation, while the error decreases during daytime, approaching zero around 17:00 as environmental temperatures rise and air exchange likely increases. This behaviour is consistent with internal heat dissipation or self-heating. The relative impact of a sensor’s internal heat becomes more significant when the gradient between sensor and environment is high and convective cooling (ventilation) is low. We therefore conclude that self-heating is a contributing factor to the observed temperature differences.

725 Because the SEN55 measures particles under these self-heated conditions, the internal RH is lower than the external ambient RH. Therefore, the RH reported by the SEN55 is the more accurate predictor hygroscopic growth occurring inside the sensor’s measurement chamber.

C.2 Representativeness of meteorological conditions

730 Under outdoor conditions, measurements for precision were conducted between 31-12-2024 and 19-09-2025. Outdoor filter measurements were conducted between 13-04-2025 and 31-12-2024. Figure C3 shows daily and hourly averaged RH and T measured at location Outdoor 1 for a full year (25-12-2024–25-12-2025), and boxplots of hourly averages for the full year, precision measurement and filter measurement periods. The measurements are taken from two other sensors with BME280 relative humidity and temperature sensor. Since we focus here only on the values on average during the different periods

735 (rather than the absolute values), we do not present validation data of the BME280.

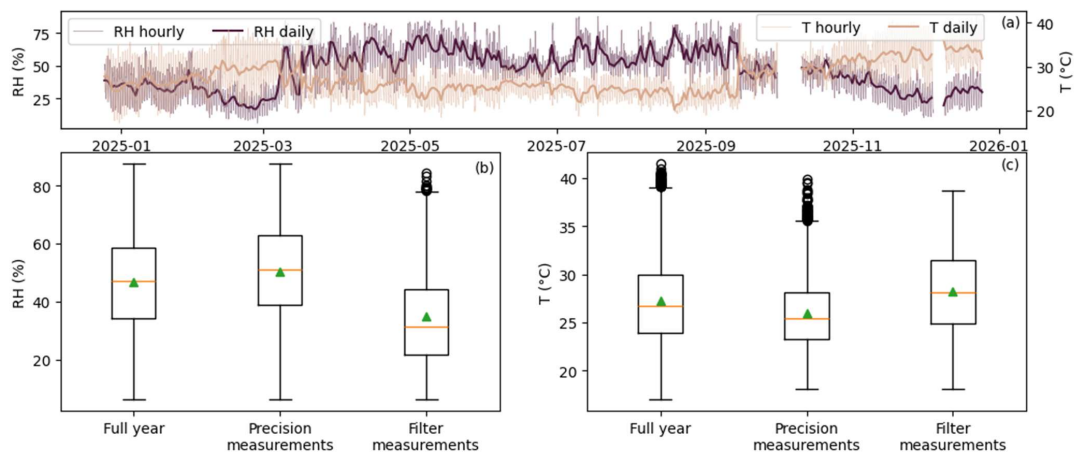


Figure C3: Temperature (T) and relative humidity (RH) for a full year (a), and boxplots of hourly values of RH (b) and T (c). The boxplots show values of the full year, of only those during precision measurements, and only those during filter measurements.

The full year average relative humidity and temperature were respectively 47 % and 27 °C. During precision measurements, this was respectively 50 % and 26 °C, while during filter measurements this was respectively 35 % and 28 °C. On average, filter measurements have been under warmer and dryer conditions. During filter measurements, however, there have also been more humid moments: hourly averages ranged up to 80 %.



Appendix D Gravimetry and sensor measurements

D.1 Phase 1 comparison of two locations

745 Figure D1 shows the daily trend for SEN1 phase 1 measurements of the two locations (Outdoor 1 and Outdoor 2), as well as boxplots of hourly averages.

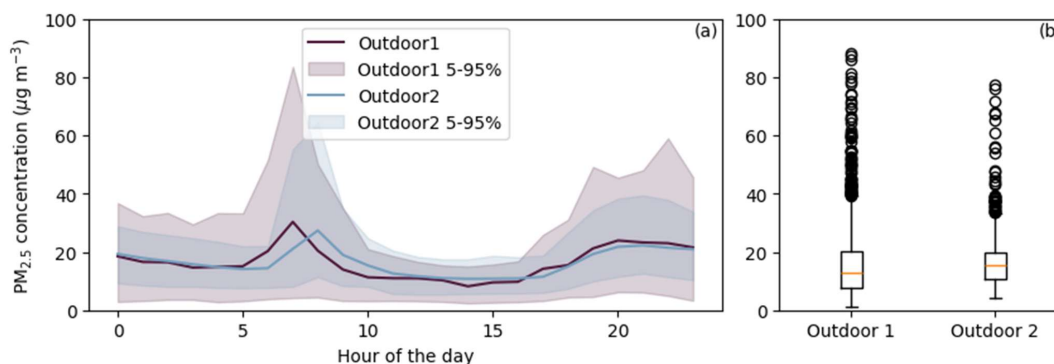


Figure D1: SEN1 PM_{2.5} measurements at locations Outdoor 1 and 2 per hour of the day (a), and boxplots of hourly averages (b). For Outdoor 1, six of the total 1523 hourly averages were higher than 100 µg/m³.

750 Phase 1 measured concentrations of Outdoor 1 and 2 were in the same order of magnitude. The higher variability observed at Outdoor 1 compared to Outdoor 2 can be attributed to the outdoor measurement setting at Outdoor 1, which allows for a more immediate response to environmental changes. We do however assume that particle compositions and concentrations at both locations are comparable enough to use all phase 1 data together.

D.2 Sensor versus gravimetry measurements

755 Figure D2 shows all outdoor sensor versus gravimetry measurements. Table D1 shows results of WLS regression with intercept for these measurements.

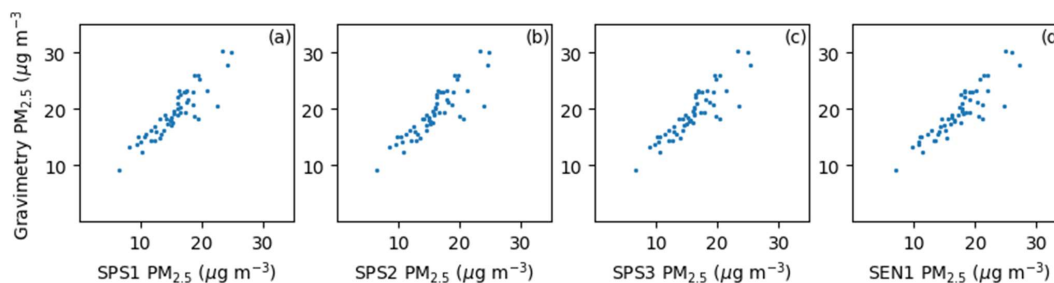


Figure D2: Sensor versus gravimetry PM_{2.5} concentrations under outdoor conditions.

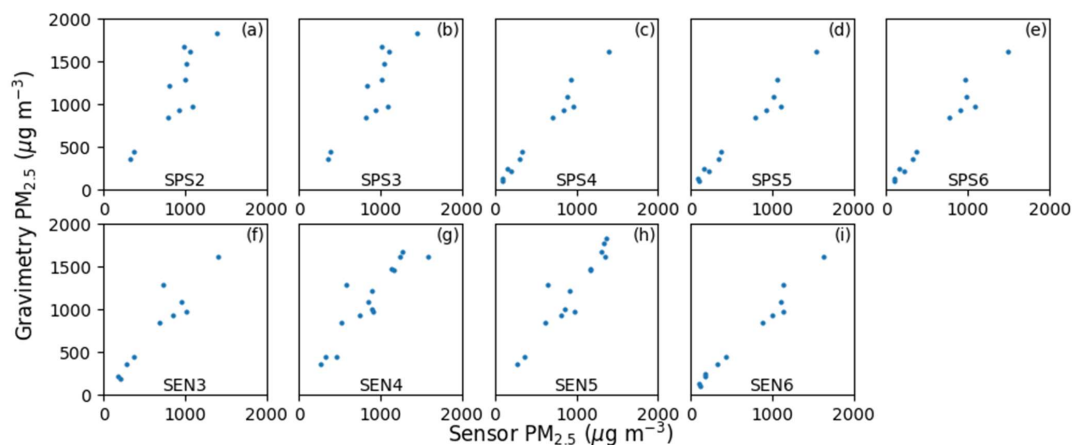


760 **Table D1: Quality metrics under outdoor conditions for PM_{2.5} sensor measurements (per ID) in comparison to gravimetric measurements: Weighted Least Squares (WLS) slope (S) and intercept (I) with 95 % confidence interval (CI) and R², and root mean square error (RMSE) after correction for S and I.**

ID	N	WLS			RMSE ($\mu\text{g m}^{-3}$)
		S [CI]	I [CI]	(R ²)	
SPS_1	53	0.97 [0.86–1.09]	3.8 [2.1–5.5]	(0.85)	1.9
SPS_2	53	0.93 [0.81–1.06]	4.1 [2.2–5.9]	(0.81)	2.1
SPS_3	53	0.94 [0.82–1.06]	3.9 [2.1–5.7]	(0.83)	2.0
SEN_1	53	0.90 [0.79–1.00]	3.5 [1.8–5.3]	(0.84)	1.9

The RMSE for correction with slope and intercept has a slight improvement (slope only: 2.1–2.3; slope and intercept: 1.9–2.1). Given however that orthogonal regression gives only significant slopes (see Table 5), that the NIOSH accuracy error only accounts for a possible bias similar to a slope, and that a slope-only correction is physically more plausible (assuming the reference is the truth, a positive intercept implies that the sensors never measure below 3.5, but this is not the case), in our main analysis we present WLS with slope only.

765 Figure D3 shows all indoor sensor versus gravimetry measurements. Table D2 shows results of WLS regression with intercept for these measurements.



770 **Figure D3: Sensor versus gravimetry PM_{2.5} concentrations under indoor conditions.**

Table D2: Quality metrics under indoor conditions for PM_{2.5} sensor measurements (per ID) in comparison to gravimetric measurements: Weighted Least Squares (WLS) slope (S) and intercept (I) with 95 % confidence interval (CI) and R², and root mean square error (RMSE) after correction for S and I.

ID	N	WLS			RMSE ($\mu\text{g m}^{-3}$)
		S [CI]	I [CI]	(R ²)	
SEN_3	10	1.18 [0.92–1.44]	-27 [-115–60]	(0.93)	157
SEN_4	15	1.18 [0.92–1.43]	43 [-107–193]	(0.89)	191



SEN_5	14	1.22 [1.03–1.42]	19 [-106–143] (0.94)	155
SPS_2	11	1.25 [0.89–1.60]	-44 [-269–180] (0.87)	246
SPS_3	11	1.24 [0.90–1.58]	-61 [-276–154] (0.89)	232
SPS_4	12	1.15 [1.01–1.30]	10 [-18–39] (0.97)	77
SPS_5	12	1.02 [0.88–1.15]	17 [-12–46] (0.97)	81
SPS_6	12	1.06 [0.92–1.20]	12 [-17–42] (0.97)	93
SEN_6	12	0.98 [0.86–1.10]	12 [-16–39] (0.97)	70
All SPS30	58	1.11 [1.05–1.18]	8 [-9–25] (0.95)	183
All SEN55	51	1.17 [1.09–1.25]	-11 [-38–17] (0.94)	186

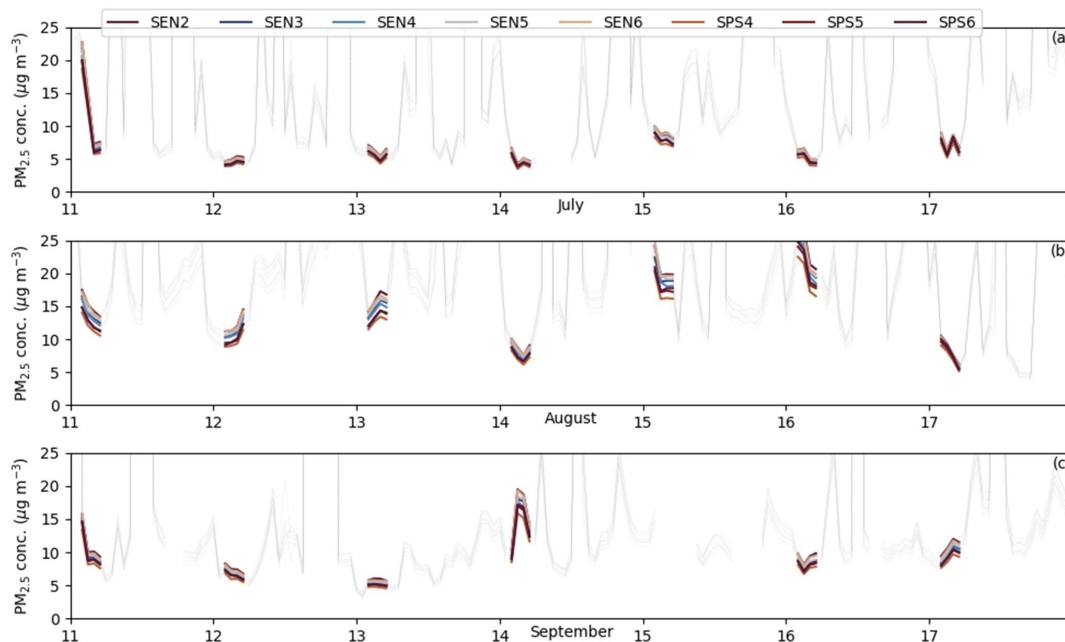
775 In all cases, the 95 % CI of the intercept includes 0. The RMSE with slope only for all SPS30 and SEN55 combined is 180 and 186 $\mu\text{g m}^{-3}$, while that of slope and intercept is virtually the same (183 and 186 $\mu\text{g m}^{-3}$). Additionally, given that the NIOSH accuracy error only accounts for a possible bias similar to a slope, and that a slope-only correction is physically more plausible, in our main analysis we present WLS with slope only.



780 Appendix E High value sensitivity analysis

E.1 Precision around high concentration measurements

At location Residence there were regular high-concentration events in the evenings. In the night-time, concentration became low again. Figure E1 shows for three weeks across the location's measurement period the concentration, with those night-time concentrations highlighted.



785

Figure E1: Hourly average concentration for eight sensors at location Residence, three weeks across the measurement period. Measurements between 2:00–6:00 are highlighted, and y-axis limits are optimized for those concentrations only.

Across the whole measurement period, after high-concentration events eight sensors measured similar concentrations. The sensors could still register low concentrations with high precision.

790 E.2 Cutoff occurrences

The SEN55 truncates all values beyond $6553.4 \mu\text{g m}^{-3}$ to that maximum value (see section 2.2.1), while the SPS30 reports higher values. Table E1 shows the number of data periods that had or had not one or more of these maximum measurements, for two sensor pairs: SPS4 with SEN3 and SPS6 with SEN6.



795 **Table E1: Contingency tables of occurrences beyond and below the SEN55 PM_{2.5} cut-off, for two SPS30/SEN55 sensor pairs, for hourly and 10-minute periods. Data periods that contain raw data with at least one value $\geq 6553.4 \mu\text{g m}^{-3}$ are classified as beyond the cut-off.**

		Hour periods			10-minute periods		
		SEN3	SEN3	Total	SEN3	SEN3	Total
		$6553.4 \mu\text{g m}^{-3}$	$< 6553.4 \mu\text{g m}^{-3}$		$6553.4 \mu\text{g m}^{-3}$	$< 6553.4 \mu\text{g m}^{-3}$	
SPS4	$\geq 6553.4 \mu\text{g m}^{-3}$	80	12	92	139	29	168
	$< 6553.4 \mu\text{g m}^{-3}$	10	1835	1845	29	11607	11636
	Total	90	1847	1937	168	11636	11804
		SEN6	SEN6	Total	SEN6	SEN6	Total
		$6553.4 \mu\text{g m}^{-3}$	$< 6553.4 \mu\text{g m}^{-3}$		$6553.4 \mu\text{g m}^{-3}$	$< 6553.4 \mu\text{g m}^{-3}$	
SPS6	$\geq 6553.4 \mu\text{g m}^{-3}$	109	1	110	216	6	222
	$< 6553.4 \mu\text{g m}^{-3}$	18	1886	1904	45	11995	12040
	total	127	1887	2014	261	12001	12262

The SPS4 and SPS6 measured beyond $6553.4 \mu\text{g m}^{-3}$ during respectively 92 and 110 hours, and during respectively 168 and 222 10-minute periods. Of these, during respectively 80 and 109 hours and 139 and 216 10-minute periods the collocated SEN55 registered cut-off values. A Pearson Chi-square test based on the hour- and 10-minute occurrences as shown in Table
 800 E1 resulted in all cases in a p-value $\ll 0.001$. The SEN55 cutoff-values are significantly matched to SPS30 beyond the cutoff.

E.3 Effect of concentration cutoff

Figure E2 shows scatter plots for sensors versus gravimetry measurements, for five situations of dealing with high sensor values: no cut-off (S1), truncation to $6553.4 \mu\text{g m}^{-3}$ (S2), removal beyond $6553.4 \mu\text{g m}^{-3}$ (S3), truncation to $1000 \mu\text{g m}^{-3}$ (S4) and removal beyond $1000 \mu\text{g m}^{-3}$ (S5). While sensor to gravimetric measurements without cut-off are linear, truncation or
 805 removal of high-concentration measurements leads to an increasing underestimation.

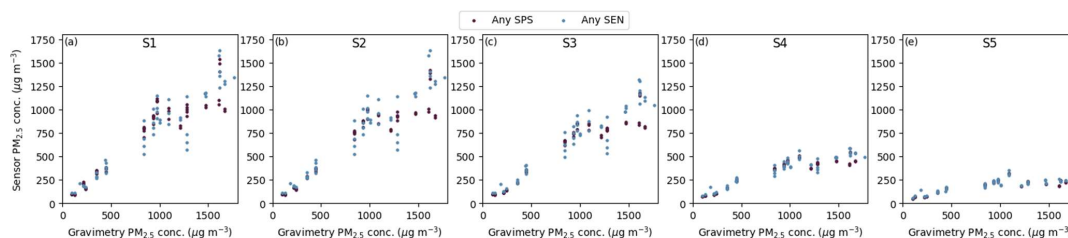


Figure E2: Sensor to gravimetry comparison for five situations (S1 through S5 in panels (a) through (e), see section 3.4.3 for details), for any SPS30 (SPS) and SEN55 (SEN).

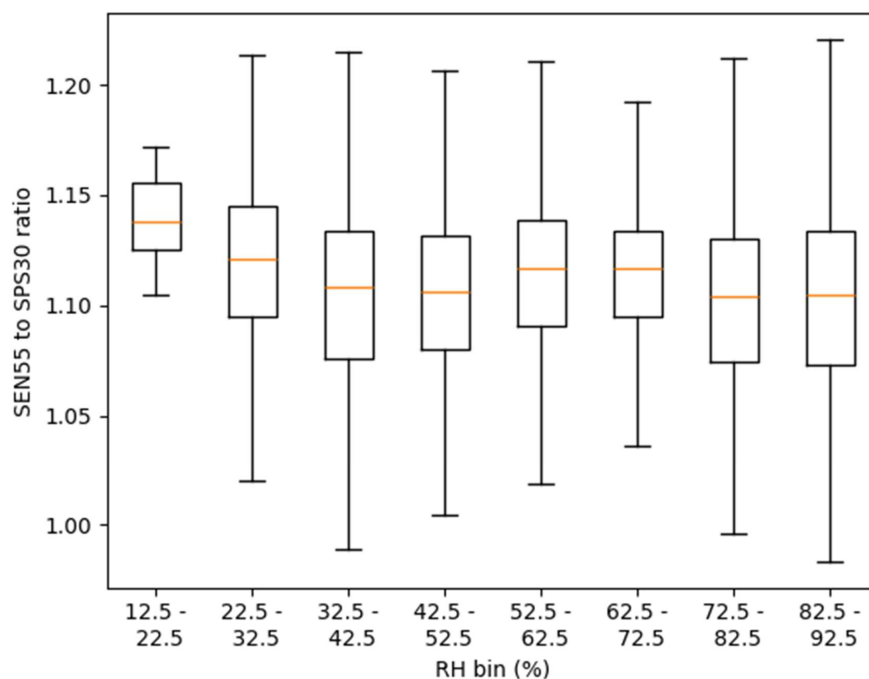
810



Appendix F Relative humidity

F.1 SEN55 to SPS30 ratio under RH changes

Figure F1 shows the ratio of SEN55 to SPS30 ten-minute averages, categorized in 10% relative humidity bins.



815 **Figure F1: SEN55 to SPS30 ratios of ten-minute averages. The boxes show 25 % to 75 % percentiles of the data (Q1 and Q3). The whiskers extent to 1.5 * (Q3 - Q1) below Q1 and above Q3.**

The average of all ratios per RH bin size varies between 1.10 and 1.14, and there is no significant trend in the ratios. An Ordinary Least Squares (OLS) regression model with $\frac{SEN55}{SPS30} = RH * slope + intercept$ gives a non-significant slope ($p = 0.699$).

There is no evidence that the SEN55 to SPS30 ratio is affected by RH, and we can therefore assume that any effect from RH

820 for the SEN55 is similar for the SPS30.

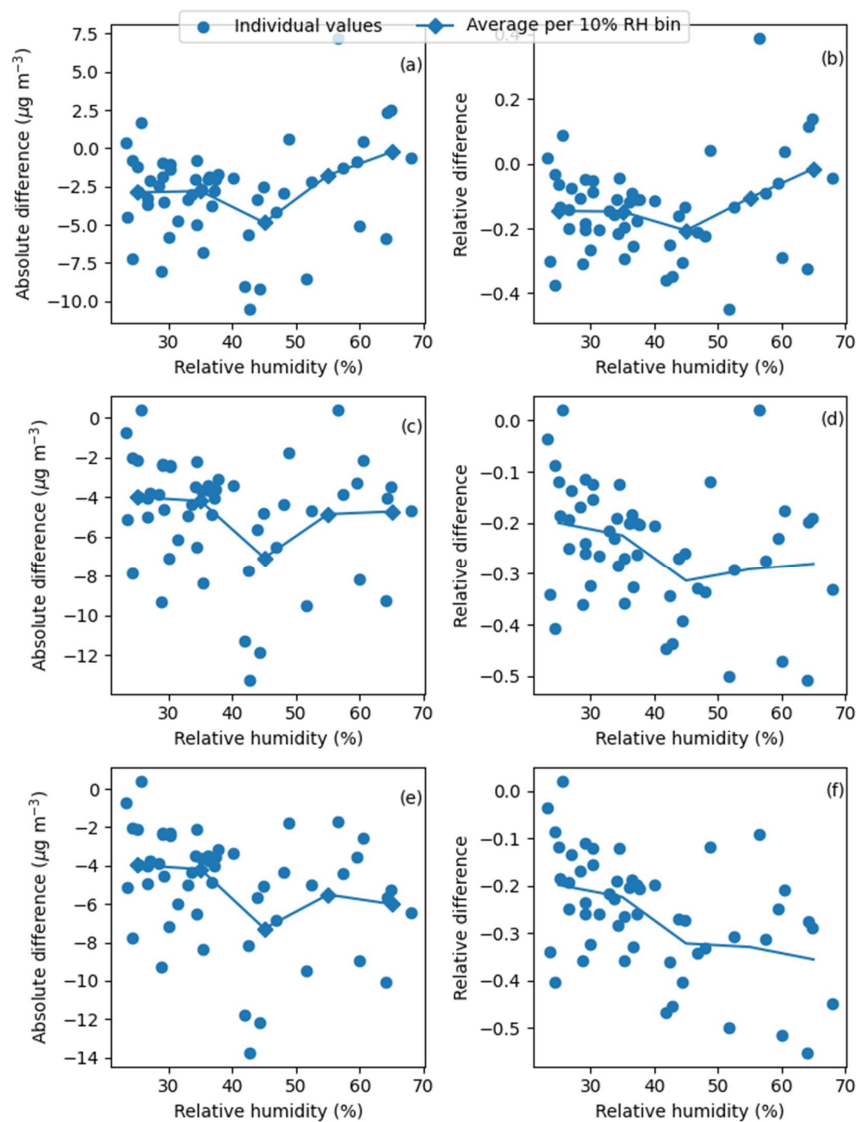
F.2 Effect of hygroscopic growth

With Eq. (5) we can calculate expected growth factors based on relative humidity GF(RH). If the SEN55 measurement data is affected by hygroscopic growth as predicted by the κ -Köhler theory, we should see an increase relative to gravimetric measurements with increasing relative humidity, and no such increase when dividing the data points by their respective growth



825 factors. Figure F2 shows the absolute and relative SEN55 to gravimetry differences (with averages per 10% relative humidity bin), for both uncorrected and GF-corrected data. We present GF-corrected data both with correction based on SEN55 RH, and RH representative for ambient RH.

Starting from the 40–50 % relative humidity bin, there is a slight upward trend towards higher relative humidities (Fig. F2 (a) and (b)). Across the whole range, the trend is not significant (p-value of slope for absolute difference to RH is 0.194; for
830 relative difference this is 0.17). A correction for GF(RH) results in a slight negative trend for the relative difference (Fig. F2 (c) and (d)). For the absolute difference after correction there is no significant trend, but for the relative difference the trend is significant (p-value of slope 0.026). Correction for growth factors results in a slight underestimation. When using RH representative for ambient temperatures (Fig. F2 (e) and (f)), the underestimation becomes more pronounced: a significant negative trend for both the absolute and relative differences ($-0.07 \mu\text{g m}^{-3}$ or -0.005 per % RH, respectively). This supports our
835 statement that the SEN55 reported RH is a better estimator than ambient RH for effects on SEN55 $\text{PM}_{2.5}$ measurements (see section C.1).



840 **Figure F2:** Differences between SEN55 and gravimetry measurements: absolute (SEN55 – gravimetry) and relative ((SEN55 – gravimetry) / gravimetry), for uncorrected values (a), (b), GF-corrected values (c), (d), and GF-corrected values based on RH corrected with Eq. (C3) (e), (f).



Appendix G Reanalysis earlier study

In our earlier work, we presented SPS30 and UPAS gravimetry measurements across three kitchens K2–K4 (Dingemanse and Tademe, 2023). Based on these measurements, we presented a slope (from Ordinary Least Squares Regression) of 0.95, a bias (B) of -8%, and an accuracy error (AE) after bias correction of 13%. The data file is available at <https://osf.io/cezqa>.

In the current study, we have two changes in our analysis: we assume orientation matters (and therefore only include collocated sensors that are oriented the same as the gravimetric instrument; see section A.3), and we use Weighted Linear Regression (WLS; see section 2.4.2). At kitchen K2, the SPS30 was oriented downward, while the UPAS was placed above it with horizontal orientation. At kitchens K3 and K4, orientation of the SPS30 and UPAS inlets was identical.

Figure G1 shows both the original analysis, as well as OLS for only kitchens K3 and K4, and WLS for kitchens K3 and K4.

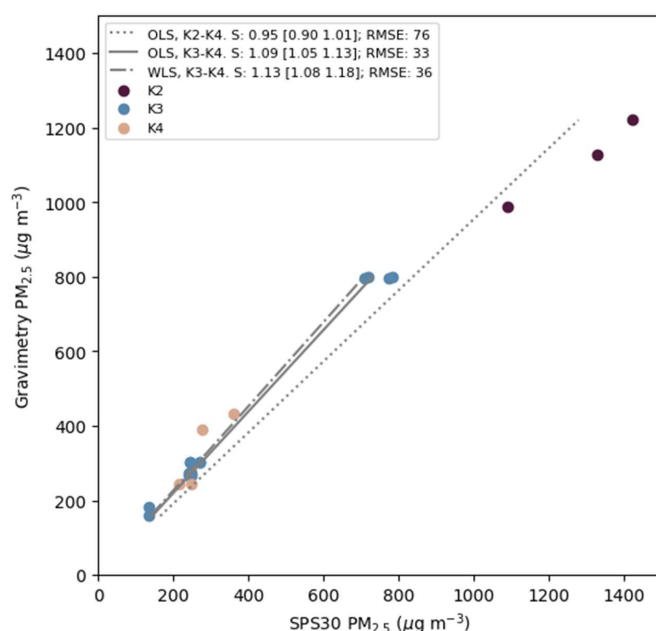


Figure G1: Measurements of collocated SPS30 and gravimetric sensors across three kitchens K2 – K4 (data from Dingemanse and Tademe (2023)), with regression model lines based on OLS regression of K2 through K4 data, OLS regression of K3 and K4 data, and WLS regression of K3 and K4 data. The legend shows the corresponding slope (S) [with 95 % confidence interval] and the root mean squared error (RMSE) after correction for the slope.

When conducting an analysis identical to our current study, we find a slope of 1.13 between the SPS30 and gravimetric measurements. B and AE after bias correction for only K3 and K4 data are -12 % and 8.5 %, respectively.



860 Appendix H Hyltemossa measurements

H.1 Measurement installation

Three SPS30 sensors (SPS7–9) and one SEN55 (SEN7) were fixed at the Hyltemossa monitoring site. At that site there is also a Palas Fidas (reference equivalent monitor). For the Palas Fidas (PF) $PM_{2.5}$ measurements, expanded uncertainty is 5.7–35 % without slope correction, and with 1.06 slope correction it is 8.5–22.4 % (CSA Group Testing UK Ltd, 2024). The PF stands
865 free at approximately 10 meters from a wooden building. The sensors were installed under a plastic box under the roof extension of that wooden building. Figure H1 shows the installation.



Figure H1: Installation of SPS30 and SEN55 sensors (left) and a Palas Fidas (right) at Hyltemossa monitoring site.

H.2 Measurements

870 Figure H2 shows data measured between May 27 and September 12, 2025.

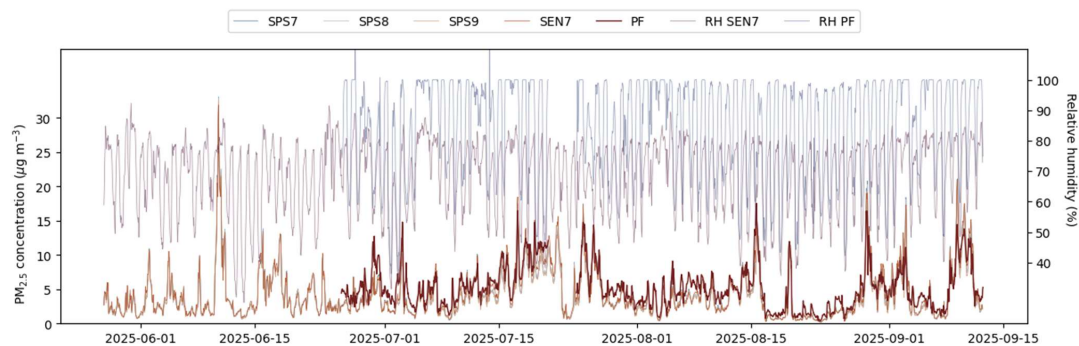




Figure H2: Hourly average measurements of PM_{2.5} and relative humidity (RH) by SPS30 and SEN55 sensors and Palas Fidas (PF) at Hyltemossa.

Apart from an event at June 10 (during which data of the Palas Fidas is missing), concentrations ranged between 0 and 20 $\mu\text{g m}^{-3}$. The relative humidity as reported by the Palas Fidas regularly capped off at 100 %, while that of the SEN55 reported continuously lower values. The lower values can be due to self-heating (see section C.1.3), but are most likely also due to a difference in measurement locations: in the open field for the PF versus next to the building for the SEN55 (see Figure H1). For evaluating the effects of RH on the PM_{2.5} concentrations (sections H.3 and H.4), we use the RH as reported by the SEN55, because both self-heating and difference in location imply that the SEN55 RH is the best representation of the RH affecting the sensor measurements.

H.2.1 Intra-sensor comparison

Table H1 shows the between-sampler uncertainty (u_{bs}) and coefficient of variation (CV) for pairs of sensors.

Table H1: u_{bs} and CV for collocated sensor pairs at Hyltemossa, Sweden.

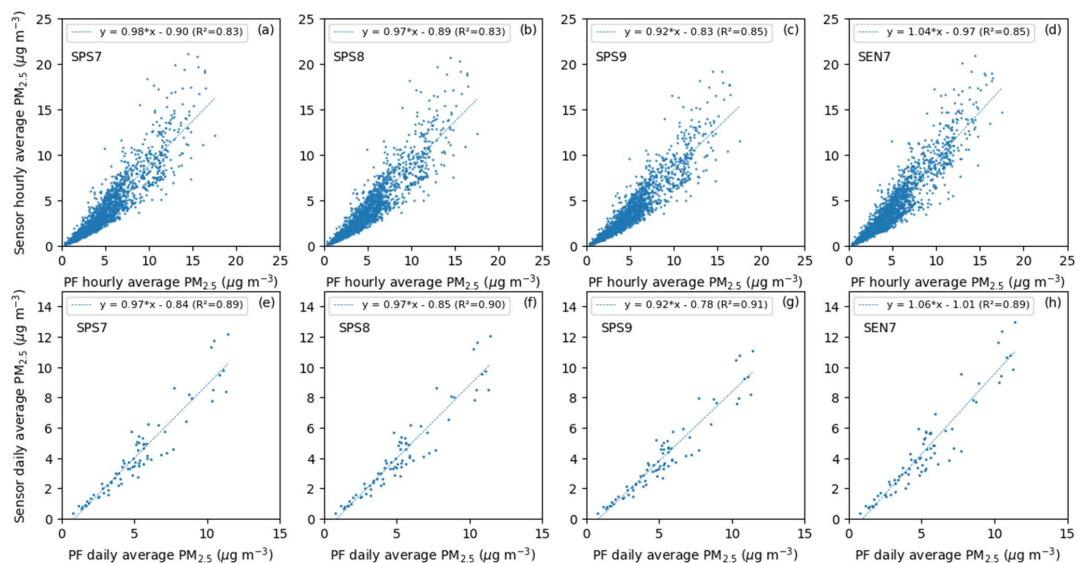
Sensor 1	Sensor 2	N	u_{bs} ($\mu\text{g m}^{-3}$)	N	CV (%)
SPS7	SPS8	107	0.04	2592	1.5
SPS7	SPS9	107	0.18	2592	3.2
SPS8	SPS9	107	0.17	2592	3.2
<i>SPS30 to SEN55 pair</i>					
SPS7	SEN7	107	0.34	2592	6.7

The three SPS30 have a high precision. The CV based on hourly averages between sensor pairs (eq. (1)) ranges from 1.5 to 3.2 %. The between sampler uncertainty (u_{bs} , eq. (2)) ranges between 0.07 to 0.18 $\mu\text{g m}^{-3}$. This is lower than the GDE, NIOSH and EPA thresholds of 10 % and 2.5 $\mu\text{g m}^{-3}$ for CV and u_{bs} , respectively.

The SPS30 to SEN55 u_{bs} and CV are also below these thresholds, but higher than those of SPS30 to SPS30. Ordinary Least Squares (OLS) regression between SEN55 and SPS30 hourly values (SPS30 = slope * SEN55 + intercept), results in a slope of 0.94 (confidence interval at 95 % 0.93–0.94). The intercept is close to zero (0.03 $\mu\text{g m}^{-3}$). The slope is significantly different from 1. The SEN55 is measuring significantly higher than the SPS30.

H.2.2 Sensor to Palas Fidas comparison

Figure H3 shows scatter plots of the PM_{2.5} measurements for the sensors versus the Palas Fidas hourly and daily averaged data.



895

Figure H3: Sensor versus Palas Fidas (PF) comparison at Hyltemossa. The line shows the model prediction resulting from Ordinary Least Squares regression.

Slopes of SPS30 to PF range from 0.92 to 0.98 (reflecting a slight underestimation of the SPS30), while that of the SEN55 is 1.04–1.06 (a slight overestimation). The difference in slopes result from the SEN55 measuring higher than the SPS30.

900 **H.3 The effect of relative humidity on SEN55 to SPS30 ratio**

Figure H4 shows the ratio of SEN55/SPS30 ten-minute averages, categorized in 10 % relative humidity bins.

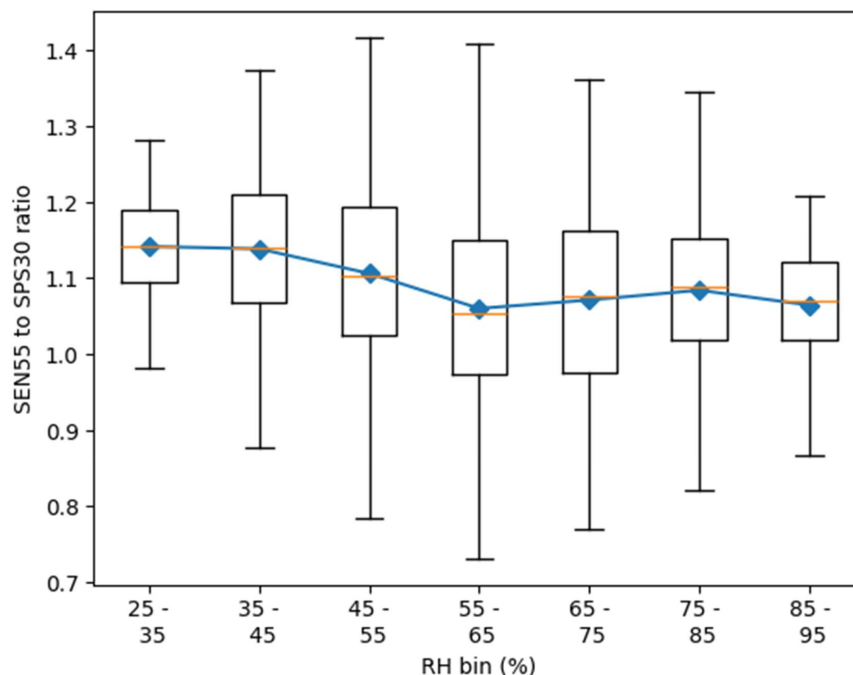


Figure H4: SEN55 to SPS30 ratios of ten-minute averages at Hyltemossa. The boxes show 25% to 75% percentiles of the data (Q1 and Q3). The whiskers extent to $1.5 * (Q3 - Q1)$ below Q1 and above Q3. The blue line and markers show the average per bin.

905 Only on the lower end of relative humidities (25–65 %) there is a downward trend. Although an OLS regression indicates a statistically significant negative slope (-6×10^{-4} per % RH, $p < 0.001$), the magnitude of the effect is small, corresponding to a change of ~4 % across the full RH range. There is no evidence for a meaningful effect of RH on the SEN55 to SPS30 ratio, and we can therefore assume that any effect from RH for the SEN55 is similar for the SPS30.

H.4 The effect of relative humidity on sensor to Palas Fidas ratio

910 Since any effect of RH is similar for the SEN55 and SPS30 (see section H.3), we only evaluate the effect of RH for the SEN55 versus the Palas Fidas measurements. With Eq. (5) we can calculate expected growth factors based on relative humidity $GF(RH)$, with a κ -value of 0.3 (as measured in rural South-Sweden) (Fors et al., 2011). If the SEN55 measurement data is affected by hygroscopic growth as predicted by the κ -Köhler theory, we should see an increase relative to gravimetric measurements with increasing relative humidity, and no such increase when dividing the data points by their respective growth

915 factors. Figure H5 shows the absolute and relative SEN55 to Palas Fidas differences (with averages per 10% relative humidity



bin), for both uncorrected and GF-corrected data. We present GF-corrected data both with corrections based on SEN55 RH, and based on PF RH.

Starting from the 50–60 % relative humidity bin, there is an upward trend towards higher relative humidities (Fig. H5 (a) and (b)). The trend across the whole range of relative humidities is significant ($0.05 \mu\text{g m}^{-3}$ change in absolute difference per % RH and 0.01 change in relative difference per % RH, $p < 0.001$), implying an estimated $3 \mu\text{g m}^{-3}$ change over the 30–90 % humidity range. When corrected with κ -Köhler, there is a slight significant downward trend in the absolute difference (Fig. H5 (c), $-0.01 \mu\text{g m}^{-3}$ change in absolute difference per % RH). In other words, the SEN55 concentrations are affected by relative humidity, at a level close to what is calculated with the κ -Köhler theory. The correction is conducted with the SEN55 measured relative humidity. When using the relative humidity as reported by the Palas Fidas, the calculated growth factors are significantly higher, resulting in an extreme underestimation (Fig. H5 (e) and (f)).

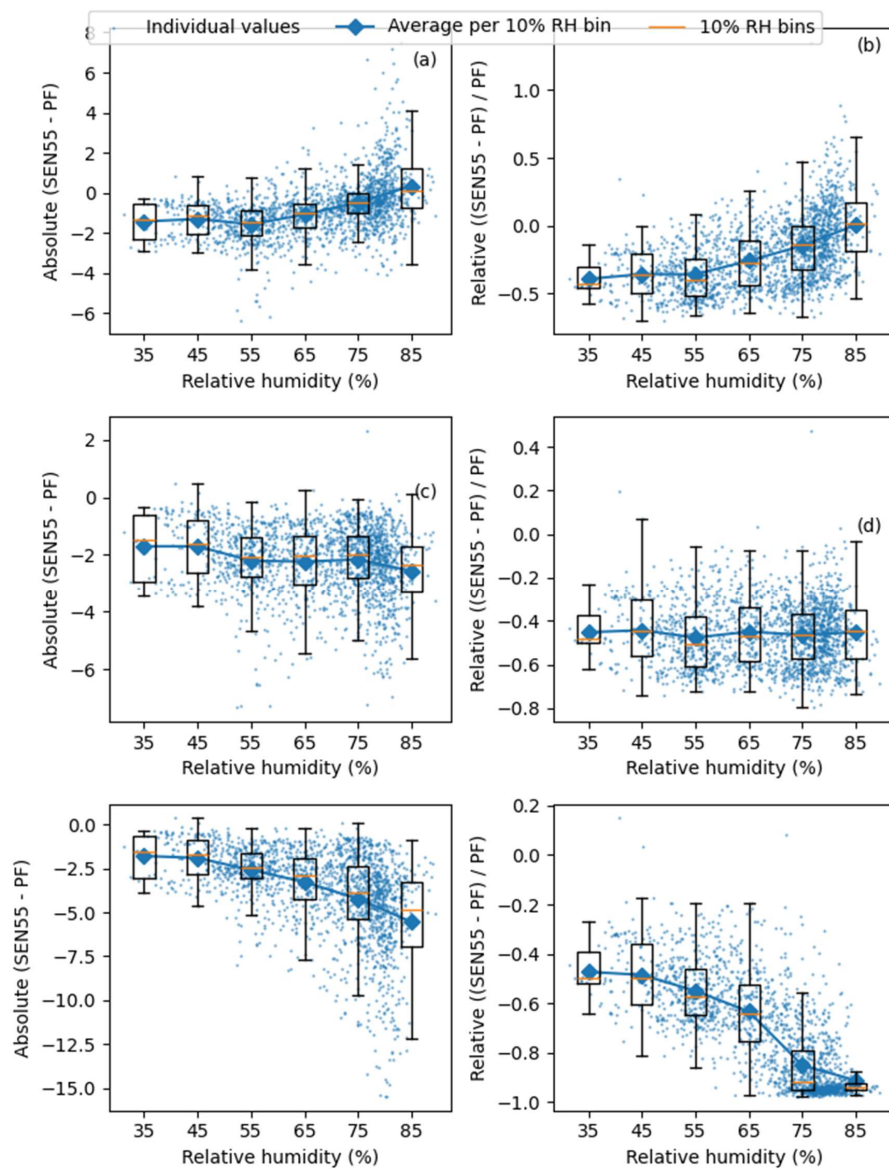


Figure H5: Differences between SEN55 and Palas Fidas (PF) hourly averages: absolute (SEN55 – PF) and relative ((SEN55 – PF) / PF), for uncorrected values (a), (b), GF-corrected values (c), (d), and GF-corrected values based on PF RH.



930 **Code and data availability**

Code and data can be downloaded from <https://doi.org/10.17605/OSF.IO/EC3T8> (Dingemanse, 2026). The code is organized in Jupyter Notebooks, see ‘Interactive computing environment’.

Interactive computing environment

All data processing code is organized in eight Jupyter Notebooks, shared on the public OSF repository
935 <https://doi.org/10.17605/OSF.IO/EC3T8> (Dingemanse, 2026). On this repository, a document is included in which usage of the Jupyter Notebooks is explained.

Author contributions

JDD was involved in all parts of the work. IGK and AHI supported data collection during Phase 1 and 2. YGD arranged the installation of instruments and supported Phase 3 data collection. NSK supported data collection during Phase 2. IGK, AHI
940 and NSK provided input to the manuscript. CI and ACE provided feedback to multiple iterations of the manuscript.

Competing interests

The authors declare that they have no conflict of interest.

Disclaimer

Copernicus Publications remains neutral with regard to jurisdictional claims made in the text, published maps, institutional
945 affiliations, or any other geographical representation in this paper. While Copernicus Publications makes every effort to include appropriate place names, the final responsibility lies with the authors. Views expressed in the text are those of the authors and do not necessarily reflect the views of the publisher.

Acknowledgements

We thank Arba Minch University WSEE year 3 and MHD year 3 2024/2025 students for conducting parts of the gravimetric
950 measurements. We are grateful to Abel Weldetinsae Kidane and Prof. Solomon Bililign for support in obtaining filter papers, and Thomas Krinke for support in obtaining a flow calibrator. We thank Asbjørn Kloppenborg for installing sensors at the ACTRIS Sweden Hyltemossa measurement station, and Erik Ahlberg for providing Hyltemossa Palas Fidas data. The Hyltemossa measurement station is funded by the Swedish Research Council and the Swedish EPA. During the preparation of this manuscript, the first author used ChatGPT (OpenAI) and Gemini (Google) to refine language clarity and improve the



955 structural flow of the technical descriptions. After using these tools, the authors reviewed and edited the content as needed and
take full responsibility for the content of the publication.

Financial support

This study was conducted without financial support.

References

- Access Sensor Technologies: Product Info Sheet Ultrasonic Personal Air Sampler (UPAS) v2.0, Fort Collins,
[https://www.accsensors.com/hubfs/Product%20Info%20Sheets/AST-UPAS%20\(v2.0\)-](https://www.accsensors.com/hubfs/Product%20Info%20Sheets/AST-UPAS%20(v2.0)-Product%20Info%20Sheet.pdf?hsLang=en)
965 [Product%20Info%20Sheet.pdf?hsLang=en](https://www.accsensors.com/hubfs/Product%20Info%20Sheets/AST-UPAS%20(v2.0)-Product%20Info%20Sheet.pdf?hsLang=en), 2024.
- Admasie, A., Kumie, A., Worku, A., and Tsehayu, W.: Household fine particulate matter (PM_{2.5}) concentrations from cooking
fuels: the case in an urban setting, Wolaita Sodo, Ethiopia, *Air Qual. Atmosphere Health*, 12, 755–763,
<https://doi.org/10.1007/s11869-019-00700-0>, 2019.
- AirNow Department of State: Addis Ababa Jacros PM_{2.5} concentration, [https://www.airnow.gov/international/us-embassies-](https://www.airnow.gov/international/us-embassies-and-consulates/#Ethiopia$Addis_Ababa_Jacros)
970 [and-consulates/#Ethiopia\\$Addis_Ababa_Jacros](https://www.airnow.gov/international/us-embassies-and-consulates/#Ethiopia$Addis_Ababa_Jacros), 2023.
- Anderson, J. O., Thundiyil, J. G., and Stolbach, A.: Clearing the Air: A Review of the Effects of Particulate Matter Air Pollution
on Human Health, *J. Med. Toxicol.*, 8, 166–175, <https://doi.org/10.1007/s13181-011-0203-1>, 2012.
- Andreae, M. O. and Rosenfeld, D.: Aerosol–cloud–precipitation interactions. Part 1. The nature and sources of cloud-active
aerosols, *Earth-Sci. Rev.*, 89, 13–41, <https://doi.org/10.1016/j.earscirev.2008.03.001>, 2008.
- 975 Baguio, A. J., Reyes, R., De Guzman, J., Rosales, M., and Hizon, J. R.: Insights from using a Wearable Air Quality Sensor
with Solar Energy Harvesting Features, in: *E3S Web of Conferences*, 03001,
<https://doi.org/10.1051/e3sconf/202563403001>, 2025.
- Blaga, R.: Field calibration and analysis of a low-cost sensor network based on the existing air quality infrastructure of a city,
<https://doi.org/10.48550/arXiv.2402.12942>, 14 March 2024.
- 980 Central Statistics Agency (Ethiopia): Population Projection of Ethiopia from all Regions at Wereda Level for 2014–2017,
Addis Ababa, <https://www.csa.gov.et>, 2013.



- Central Statistics Agency (Ethiopia): Population projection: Population Size by Sex Zone and Woreda July 2023, Addis Ababa, <https://www.statsethiopia.gov.et/wp-content/uploads/2023/08/Population-of-Zones-and-Weredas-Projected-as-of-July-2023.pdf>, 2023.
- 985 Crilley, L. R., Shaw, M., Pound, R., Kramer, L. J., Price, R., Young, S., Lewis, A. C., and Pope, F. D.: Evaluation of a low-cost optical particle counter (Alphasense OPC-N2) for ambient air monitoring, *Atmospheric Meas. Tech.*, 11, 709–720, <https://doi.org/10.5194/amt-11-709-2018>, 2018.
- CSA Group Testing UK Ltd: MCERTS Product Conformity Certificat Fidas 200, <https://www.csagroup.org/wp-content/uploads/MC16029004-1.pdf>, 2024.
- 990 CSA Group Testing UK Ltd: mCERTS Product conformity certificate SPS30 Particulate Matter Sensor, <https://www.csagroup.org/wp-content/uploads/MC20035004.pdf>, 2025a.
- CSA Group Testing UK Ltd: MCERTS Product conformity certificate Topas Airborne Particle Monitor, <https://www.csagroup.org/wp-content/uploads/MC20035004.pdf>, 2025b.
- Dingemane, J. D.: Evaluation of Three Low-Cost Particulate Matter (PM_{2.5}) Sensors for Ambient and High Exposure Conditions in Arba Minch, Ethiopia, *Ethiop. J. Water Sci. Technol.*, 4, 33–61, <https://doi.org/10.59122/134080D>, 2022.
- Dingemane, J. D.: Data and code for SPS30 SEN55 PM_{2.5} indoor outdoor validation, Arba Minch, Ethiopia, OSF [code], <https://doi.org/10.17605/OSF.IO/EC3T8>, 2026.
- Dingemane, J. D. and Tademe, A.: Developing and testing a PM_{2.5} low-cost sensor in Ethiopia under ambient and indoor air pollution conditions, *Clean Air J.*, 33, <https://doi.org/10.17159/caj/2023/33/2.16488>, 2023.
- 1000 Enyew, H. D., Hailu, A. B., and Mereta, S. T.: Kitchen fine particulate matter (PM_{2.5}) concentrations from biomass fuel use in rural households of Northwest Ethiopia, *Front. Public Health*, 11, <https://doi.org/10.3389/fpubh.2023.1241977>, 2023.
- European Commission: Guide to the demonstration of equivalence of ambient air monitoring methods, European Commission, https://www.academia.edu/65705447/Guide_to_the_Demonstration_of_Equivalence_of_Ambient_Air_Monitoring_Methods, 2010.
- 1005 European Union: Directive 2008/50/EC, , 2008/50/EC, <http://data.europa.eu/eli/dir/2008/50/2015-09-18/eng>, 2015.
- Findlay, M., Peaslee, D., Stetter, J. R., Waller, S., and Smallridge, A.: Distributed Sensors for Wildfire Early Warnings, *J. Electrochem. Soc.*, 169, 020553, <https://doi.org/10.1149/1945-7111/ac5344>, 2022.
- Fors, E. O., Swietlicki, E., Svenningsson, B., Kristensson, A., Frank, G. P., and Sporre, M.: Hygroscopic properties of the ambient aerosol in southern Sweden – a two year study, *Atmospheric Chem. Phys.*, 11, 8343–8361, <https://doi.org/10.5194/acp-11-8343-2011>, 2011.
- 1010 Gäbel, P., Koller, C., Hertig, E., Gäbel, P., Koller, C., and Hertig, E.: Development of Air Quality Boxes Based on Low-Cost Sensor Technology for Ambient Air Quality Monitoring, *Sensors*, 22, <https://doi.org/10.3390/s22103830>, 2022.
- Gabriel, M. and Auer, T.: LSTM Deep Learning Models for Virtual Sensing of Indoor Air Pollutants: A Feasible Alternative to Physical Sensors, *Buildings*, 13, 1684, <https://doi.org/10.3390/buildings13071684>, 2023.



- 1015 Hassani, A., Castell, N., Watne, Å. K., and Schneider, P.: Citizen-operated mobile low-cost sensors for urban PM_{2.5} monitoring: field calibration, uncertainty estimation, and application, *Sustain. Cities Soc.*, 95, 104607, <https://doi.org/10.1016/j.scs.2023.104607>, 2023.
- Hofman, J., Nikolaou, M., Shantharam, S. P., Stroobants, C., Weijs, S., and La Manna, V. P.: Distant calibration of low-cost PM and NO₂ sensors; evidence from multiple sensor testbeds, *Atmospheric Pollut. Res.*, 13, 101246, 1020 <https://doi.org/10.1016/j.apr.2021.101246>, 2022a.
- Hofman, J., Do, T. H., Qin, X., Bonet, E. R., Philips, W., Deligiannis, N., and La Manna, V. P.: Spatiotemporal air quality inference of low-cost sensor data: Evidence from multiple sensor testbeds, *Environ. Model. Softw.*, 149, 105306, <https://doi.org/10.1016/j.envsoft.2022.105306>, 2022b.
- Hofman, J., Lazarov, B., Stroobants, C., Elst, E., Smets, I., Poppel, M. V., Hofman, J., Lazarov, B., Stroobants, C., Elst, E., 1025 Smets, I., and Poppel, M. V.: Portable Sensors for Dynamic Exposure Assessments in Urban Environments: State of the Science, *Sensors*, 24, <https://doi.org/10.3390/s24175653>, 2024.
- Hong, G.-H., Le, T.-C., Tu, J.-W., Wang, C., Chang, S.-C., Yu, J.-Y., Lin, G.-Y., Aggarwal, S. G., and Tsai, C.-J.: Long-term evaluation and calibration of three types of low-cost PM_{2.5} sensors at different air quality monitoring stations, *J. Aerosol Sci.*, 157, 105829, <https://doi.org/10.1016/j.jaerosci.2021.105829>, 2021.
- 1030 Hu, W., Downward, G. S., Reiss, B., Xu, J., Bassig, B. A., Hosgood, H. D. I., Zhang, L., Seow, W. J., Wu, G., Chapman, R. S., Tian, L., Wei, F., Vermeulen, R., and Lan, Q.: Personal and Indoor PM_{2.5} Exposure from Burning Solid Fuels in Vented and Unvented Stoves in a Rural Region of China with a High Incidence of Lung Cancer, *Environ. Sci. Technol.*, 48, 8456–8464, <https://doi.org/10.1021/es502201s>, 2014.
- IET: Mettler Analytical Balance AE240 Dual Range Balance Data Sheet, ,
1035 https://www.ietltd.com/pdf_datasheets/Mettler%20AE240%20Data%20Sheet.pdf, n.d.
- Karagulian, F.: New Challenges in Air Quality Measurements, in: *Air Quality Networks*, edited by: De Vito, S., Karatzas, K., Bartonova, A., and Fattoruso, G., Springer International Publishing, Cham, 1–18, https://doi.org/10.1007/978-3-031-08476-8_1, 2023.
- Karagulian, F., Barbieri, M., Kotsev, A., Spinelle, L., Gerboles, M., Lagler, F., Redon, N., Crunaire, S., and Borowiak, A.: 1040 Review of the Performance of Low-Cost Sensors for Air Quality Monitoring, *Atmosphere*, 10, 506, <https://doi.org/10.3390/atmos10090506>, 2019.
- Kreidenweis, S. M. and Asa-Awuku, A.: Aerosol hygroscopicity: Particle water content and its role in atmospheric processes, *Treatise Geochem.*, 331–361, <https://doi.org/10.1016/B978-0-08-095975-7.00418-6>, 2014.
- Kumar, P., Khare, M., Harrison, R. M., Bloss, W. J., Lewis, A., Coe, H., and Morawska, L.: New directions: air pollution 1045 challenges for developing megacities like Delhi, *Atmos. Environ.*, 122, 657–661, <https://doi.org/10.1016/j.atmosenv.2015.10.032>, 2015.
- Li, J., Mattewal, S. K., Patel, S., and Biswas, P.: Evaluation of Nine Low-cost-sensor-based Particulate Matter Monitors, *Aerosol Air Qual. Res.*, 20, 254–270, <https://doi.org/10.4209/aaqr.2018.12.0485>, 2020.



- Liu, H.-Y., Schneider, P., Haugen, R., Vogt, M., Liu, H.-Y., Schneider, P., Haugen, R., and Vogt, M.: Performance Assessment
1050 of a Low-Cost PM_{2.5} Sensor for a near Four-Month Period in Oslo, Norway, *Atmosphere*, 10,
<https://doi.org/10.3390/atmos10020041>, 2019.
- Mahajan, S.: Design and development of an open-source framework for citizen-centric environmental monitoring and data
analysis, *Sci. Rep.*, 12, 14416, <https://doi.org/10.1038/s41598-022-18700-z>, 2022.
- Maji, K. J., Arora, M., and Dikshit, A. K.: Burden of disease attributed to ambient PM_{2.5} and PM₁₀ exposure in 190 cities in
1055 China, *Environ. Sci. Pollut. Res.*, 24, 11559–11572, <https://doi.org/10.1007/s11356-017-8575-7>, 2017.
- Malings, C., Tanzer, R., Haurlyliuk, A., Saha, P. K., Robinson, A. L., Presto, A. A., and Subramanian, R.: Fine particle mass
monitoring with low-cost sensors: Corrections and long-term performance evaluation, *Aerosol Sci. Technol.*, 54, 160–174,
<https://doi.org/10.1080/02786826.2019.1623863>, 2020.
- Mekonnen, E. F.: Assessing the Impact of Lakes Abaya and Chamo on Regional Climate: Insights from WRF-Chemistry
1060 Simulations in Arba Minch, Ethiopia, *Asian J. Res. Biol.*, 7, 60–70, <https://doi.org/10.56557/ajrib/2024/v7i1139>, 2024.
- Morawska, L., Thai, P. K., Liu, X., Asumadu-Sakyi, A., Ayoko, G., Bartonova, A., Bedini, A., Chai, F., Christensen, B., and
Dunbabin, M.: Applications of low-cost sensing technologies for air quality monitoring and exposure assessment: How far
have they gone?, *Environ. Int.*, 116, 286–299, <https://doi.org/10.1016/j.envint.2018.04.018>, 2018.
- Mouton, M., Malek, K. A., James, M. H., Pokhrel, R. P., Fiddler, M. N., Asa-Awuku, A. A., and Bililign, S.: The hygroscopic
1065 properties of biomass burning aerosol from Eucalyptus and cow dung under different combustion conditions, *Aerosol Sci.
Technol.*, 57, 665–677, <https://doi.org/10.1080/02786826.2023.2198587>, 2023.
- Mujan, I., Licina, D., Kljajić, M., Čulić, A., and Anđelković, A. S.: Development of indoor environmental quality index using
a low-cost monitoring platform, *J. Clean. Prod.*, 312, 127846, <https://doi.org/10.1016/j.jclepro.2021.127846>, 2021.
- Mushtaq, Z., Bangotra, P., Gautam, A. S., Sharma, M., Suman, Gautam, S., Singh, K., Kumar, Y., and Jain, P.: Satellite or
1070 ground-based measurements for air pollutants (PM_{2.5}, PM₁₀, SO₂, NO₂, O₃) data and their health hazards: which is most
accurate and why?, *Environ. Monit. Assess.*, 196, 342, <https://doi.org/10.1007/s10661-024-12462-z>, 2024.
- Nguyen, N. H., Nguyen, H. X., Le, T. T. B., and Vu, C. D.: Evaluating Low-Cost Commercially Available Sensors for Air
Quality Monitoring and Application of Sensor Calibration Methods for Improving Accuracy, *Open J. Air Pollut.*, 10, 1,
<https://doi.org/10.4236/ojap.2021.101001>, 2021.
- 1075 Park, D., Yoo, G.-W., Park, S.-H., and Lee, J.-H.: Assessment and Calibration of a Low-Cost PM_{2.5} Sensor Using Machine
Learning (HybridLSTM Neural Network): Feasibility Study to Build an Air Quality Monitoring System, *Atmosphere*, 12,
1306, <https://doi.org/10.3390/atmos12101306>, 2021a.
- Park, Y. M., Sousan, S., Streuber, D., and Zhao, K.: GeoAir—A Novel Portable, GPS-Enabled, Low-Cost Air-Pollution
Sensor: Design Strategies to Facilitate Citizen Science Research and Geospatial Assessments of Personal Exposure, *Sensors*,
1080 21, 3761, <https://doi.org/10.3390/s21113761>, 2021b.



- Penchala, A., Patra, A. K., Mishra, N., and Santra, S.: Field calibration and performance evaluation of low-cost sensors for monitoring airborne PM in the occupational mining environment, *J. Aerosol Sci.*, 184, 106519, <https://doi.org/10.1016/j.jaerosci.2024.106519>, 2025.
- Petters, M. D. and Kreidenweis, S. M.: A single parameter representation of hygroscopic growth and cloud condensation nucleus activity, *Atmospheric Chem. Phys.*, 7, 1961–1971, <https://doi.org/10.5194/acp-7-1961-2007>, 2007.
- 1085 Rabuan, U., Mohd Nadzir, M. S., Abdullah Sham, S. Z., Izzati Wan Shaiful Bahri, S. B., Borah, J., Majumdar, S., Lei, T. M., Md Ali, S. H., A Wahab, M. I., and Mohd Yunus, N. H.: Evaluations of Low-cost Air Quality Sensors for Particulate Matter (PM 2.5) under Indoor and Outdoor Conditions., *Sens. Mater.*, 35, 2881–2895, <https://doi.org/10.18494/SAM4393>, 2023.
- Riediker, M.: Low Transmission of Coronavirus via Aerosols during Outdoor Running Races and Athletic Events, *Aerosol Air Qual. Res.*, 22, 220069, <https://doi.org/10.4209/aaqr.220069>, 2022.
- 1090 Rissler, J., Svenningsson, B., Fors, E. O., Bilde, M., and Swietlicki, E.: An evaluation and comparison of cloud condensation nucleus activity models: Predicting particle critical saturation from growth at subsaturation, *J. Geophys. Res. Atmospheres*, 115, <https://doi.org/10.1029/2010JD014391>, 2010.
- Rodríguez Rama, J. A., Presa Madrigal, L., Costafreda Musteliet, J. L., García Laso, A., Maroto Lorenzo, J., and Martín Sánchez, D. A.: Monitoring and Ensuring Worker Health in Controlled Environments Using Economical Particle Sensors, *Sensors*, 24, 5267, <https://doi.org/10.3390/s24165267>, 2024.
- 1095 Safo-Adu, G., Attiogbe, F., Emahi, I., and Ofofu, F. G.: Outdoor and indoor particle air pollution and its health consequences in African cities: New evidence and an exhortation, *Sustain. Environ.*, 9, 2265729, <https://doi.org/10.1080/27658511.2023.2265729>, 2023.
- 1100 Sensirion: Sensor Specification Statement, Sensirion AG, Staefa, Switzerland, https://sensirion.com/media/documents/B7AAA101/61653FB8/Sensirion_Partuculate_Matter_AppNotes_Specification_Statement.pdf, 2020.
- Sensirion: Datasheet SEN5x, Sensirion AG, Staefa, Switzerland, https://sensirion.com/media/documents/6791EFA0/62A1F68F/Sensirion_Datasheet_Environmental_Node_SEN5x.pdf, 2022.
- 1105 Sensirion: Datasheet SPS30, Sensirion AG, Staefa, Switzerland, https://sensirion.com/media/documents/8600FF88/64A3B8D6/Sensirion_PM_Sensors_Datasheet_SPS30.pdf, 2023.
- Shalisha, A., Bhowmick, A., and Elias, K.: Meteorological Drought Monitoring Based on Satellite CHIRPS Product over Gamo Zone, Southern Ethiopia, *Adv. Meteorol.*, 2022, 9323263, <https://doi.org/10.1155/2022/9323263>, 2022.
- 1110 Shittu, A. I., Pringle, K. J., Arnold, S. R., Pope, R. J., Graham, A. M., Reddington, C., Rigby, R., and McQuaid, J. B.: Performance evaluation of Atmotube PRO sensors for air quality measurements in an urban location, *Atmospheric Meas. Tech.*, 18, 817–828, <https://doi.org/10.5194/amt-18-817-2025>, 2025.
- Sousan, S., Regmi, S., and Park, Y. M.: Laboratory Evaluation of Low-Cost Optical Particle Counters for Environmental and Occupational Exposures, *Sensors*, 21, 4146, <https://doi.org/10.3390/s21124146>, 2021.



- 1115 Sousan, S., Streuber, D., Park, Y. M., Coombs, V., Pender, J., and Soule, E.: Evaluation of low-cost aerosol and gas sensors for real-time measurements of electronic cigarette exposure, *Aerosol Sci. Technol.*, 57, 153–164, <https://doi.org/10.1080/02786826.2022.2154192>, 2023.
- Streuber, D., Park, Y. M., and Sousan, S.: Laboratory and Field Evaluations of the GeoAir2 Air Quality Monitor for Use in Indoor Environments, *Aerosol Air Qual. Res.*, 22, 220119, <https://doi.org/10.4209/aaqr.220119>, 2022.
- 1120 Suriano, D. and Prato, M.: An Investigation on the Possible Application Areas of Low-Cost PM Sensors for Air Quality Monitoring, *Sensors*, 23, 3976, <https://doi.org/10.3390/s23083976>, 2023.
- Tamire, M., Kumie, A., Addissie, A., Ayalew, M., Boman, J., Skovbjerg, S., Andersson, R., Lärstad, M., Tamire, M., Kumie, A., Addissie, A., Ayalew, M., Boman, J., Skovbjerg, S., Andersson, R., and Lärstad, M.: High Levels of Fine Particulate Matter (PM_{2.5}) Concentrations from Burning Solid Fuels in Rural Households of Butajira, Ethiopia, *Int. J. Environ. Res. Public Health*, 18, <https://doi.org/10.3390/ijerph18136942>, 2021.
- 1125 Tefera, W., Kumie, A., Berhane, K., Gilliland, F., Lai, A., Sricharoenvech, P., Patz, J., Samet, J., and Schauer, J. J.: Source Apportionment of Fine Organic Particulate Matter (PM_{2.5}) in Central Addis Ababa, Ethiopia, *Int. J. Environ. Res. Public Health*, 18, 11608, <https://doi.org/10.3390/ijerph182111608>, 2021.
- Tryner, J., Mehaffy, J., Miller-Lionberg, D., and Volckens, J.: Effects of aerosol type and simulated aging on performance of low-cost PM sensors, *J. Aerosol Sci.*, 150, 105654, <https://doi.org/10.1016/j.jaerosci.2020.105654>, 2020.
- 1130 TUV SUD: Type Test Report Sampling System for Standard gravimetric measurement method for the determination of the PM₁₀ or PM_{2.5} mass concentration of suspended matter, https://www.leckel.de/wp-content/uploads/2025/06/3969062_Leckel-SEQ-Summary-preliminary.pdf, 2025.
- Vogt, M., Schneider, P., Castell, N., Hamer, P., Vogt, M., Schneider, P., Castell, N., and Hamer, P.: Assessment of Low-Cost Particulate Matter Sensor Systems against Optical and Gravimetric Methods in a Field Co-Location in Norway, *Atmosphere*, 12, <https://doi.org/10.3390/atmos12080961>, 2021.
- 1135 Wang, Z., Chen, Z., Shahid, I., Asif, Z., Haghghat, F., Wang, Z., Chen, Z., Shahid, I., Asif, Z., and Haghghat, F.: Indoor Air Quality Assessment Through IoT Sensor Technology: A Montreal–Qatar Case Study, *Atmosphere*, 16, <https://doi.org/10.3390/atmos16050574>, 2025.
- 1140 Wesseling, J., Hendricx, W., de Ruiten, H., van Ratingen, S., Drukker, D., Huitema, M., Schouwenaar, C., Janssen, G., van Aken, S., Smeenk, J. W., Hof, A., and Tielemans, E.: Assessment of PM_{2.5} Exposure during Cycle Trips in The Netherlands Using Low-Cost Sensors, *Int. J. Environ. Res. Public Health*, 18, 6007, <https://doi.org/10.3390/ijerph18116007>, 2021.
- Wesseling, J., Drukker, D., Gressent, A., Janssen, S., Joassin, P., Lenartz, F., van Ratingen, S., Rodrigues, V., Sousa, J., and Thunis, P.: Using synthetic data to benchmark correction methods for low-cost air quality sensor networks, *Air Qual. Atmosphere Health*, 17, 979–996, <https://doi.org/10.1007/s11869-023-01493-z>, 2024.
- 1145 World Health Organization: WHO global air quality guidelines. Particulate matter (PM_{2.5} and PM₁₀), ozone, nitrogen dioxide, sulfur dioxide and carbon monoxide, World Health Organization, Geneva, <https://apps.who.int/iris/handle/10665/345329>, 2021.



- Ambient (outdoor) air pollution: [https://www.who.int/news-room/fact-sheets/detail/ambient-\(outdoor\)-air-quality-and-health](https://www.who.int/news-room/fact-sheets/detail/ambient-(outdoor)-air-quality-and-health),
1150 last access: 24 February 2026.
- Household air pollution: <https://www.who.int/news-room/fact-sheets/detail/household-air-pollution-and-health>, last access:
24 February 2026.
- World Meteorological Organization: Guide to Meteorological Instruments and Methods of Observation, Seventh edition.,
World Meteorological Organization, Geneva, <https://wmo.int/guide-instruments-and-methods-of-observation-wmo-no-8-0>,
1155 2008.
- Zaid, M. M., Amoah, N., Kakoria, A., Wang, Y., and Xu, G.: Advancing occupational health in mining: investigating low-cost
sensors suitability for improved coal dust exposure monitoring, *Meas. Sci. Technol.*, 35, 025128,
<https://doi.org/10.1088/1361-6501/ad0c2e>, 2023.
- Zieger, P., Fierz-Schmidhauser, R., Weingartner, E., and Baltensperger, U.: Effects of relative humidity on aerosol light
1160 scattering: results from different European sites, *Atmospheric Chem. Phys.*, 13, 10609–10631, <https://doi.org/10.5194/acp-13-10609-2013>, 2013.
- Zusman, M., Schumacher, C. S., Gasset, A. J., Spalt, E. W., Austin, E., Larson, T. V., Carvlin, G., Seto, E., Kaufman, J. D.,
and Sheppard, L.: Calibration of low-cost particulate matter sensors: Model development for a multi-city epidemiological
study, *Environ. Int.*, 134, 105329, <https://doi.org/10.1016/j.envint.2019.105329>, 2020.
- 1165